

MSB81-WIC-0033

MSB81-WIC-0033

2

Technical Report

DAI11234

TIME-VARYING RCS MODELING ALGORITHMS

December 1981

DTIC
ELECTE
FEB 22 1982
B

THE VIEWS, OPINIONS, AND/OR FINDINGS CONTAINED IN THIS REPORT ARE THOSE OF THE AUTHOR(S) AND SHOULD NOT BE CONSTRUED AS AN OFFICIAL DEPARTMENT OF THE ARMY POSITION, POLICY, OR DECISION, UNLESS SO DESIGNATED BY OTHER OFFICIAL DOCUMENTATION.

DISTRIBUTION STATEMENT A

Approved for public release
Distribution Unlimited

 **TELEDYNE
BROWN ENGINEERING**

Cummings Research Park • Huntsville, Alabama 35807

81 12 14 008

TECHNICAL REPORT
MSB81-WIC-0033

TIME-VARYING RCS MODELING ALGORITHMS

Edited by
W. J. Gruner

December 1981

Prepared for
BALLISTIC MISSILE DEFENSE SYSTEMS COMMAND
DEPARTMENT OF THE ARMY
HUNTSVILLE, ALABAMA

Contract No. DASG60-79-C-0094

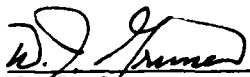
Prepared by
SYSTEMS DIVISION
TELEDYNE BROWN ENGINEERING
HUNTSVILLE, ALABAMA

THE VIEWS, OPINIONS, AND/OR FINDINGS CONTAINED IN
THIS REPORT ARE THOSE OF THE AUTHOR(S) AND SHOULD
NOT BE CONSTRUED AS AN OFFICIAL DEPARTMENT OF THE
ARMY POSITION, POLICY, OR DECISION, UNLESS SO DESIG-
NATED BY OTHER OFFICIAL DOCUMENTATION.

409

ABSTRACT

Teledyne Brown Engineering (TBE) has developed high-fidelity exoatmospheric time-varying radar cross section (RCS) models for use in the Warning Information Correlation (WIC) threat development effort. These models have been developed for the objects of six USSR ICBM and SLBM weapon systems. This report describes the five TBE developed time-varying RCS modeling algorithms that were utilized for these models. Part of the validation of these models consisted of comparisons of selected discrimination signatures calculated from model and recorded data. The definition of these signatures is also presented.


W. J. Gruner
Editor

APPROVED:


L. K. Montgomery, Jr.
Manager
Radar Systems Branch

RE: Classified Reference, Distribution
Unlimited
No change in Distribution Statement per
Lt. W.D. Peck, ESD/XRWT.

SEARCHED	INDEXED
SERIALIZED	FILED
PER LETTER	
A	

TABLE OF CONTENTS

	Page
1. INTRODUCTION	1-1
2. RCS MODEL ALGORITHMS DEVELOPMENT	2-1
2.1 SPB Algorithm	2-1
2.2 MSPB Algorithm	2-2
2.3 CORS Algorithm	2-2
2.4 SARP Algorithm	2-2
2.5 SARP2 Algorithm	2-3
2.6 MSARP Algorithm	2-3
3. RCS MODEL VALIDATION	3-1
3.1 RCS Discrimination Signatures	3-1
3.2 Noise Effects on Discrimination Signature	3-1
REFERENCES	R-1
APPENDIX A. STATIC PATTERN BASED (SPB) TIME VARYING RCS ALGORITHM	A-1
APPENDIX B. MODIFIED STATIC PATTERN BASED (MSPB) TIME VARYING RCS ALGORITHM	B-1
APPENDIX C. CORRELATED STATISTICAL (CORS) TIME VARYING RCS ALGORITHM	C-1
APPENDIX D. SINUSOIDS AND RANDOM PROCESS (SARP) TIME VARYING RCS ALGORITHM	D-1
APPENDIX E. MODIFIED SINUSOIDS AND RANDOM PROCESS (MSARP) TIME VARYING RCS ALGORITHM	E-1

1. INTRODUCTION

TBE was tasked under Contract DASG60-79-C-0094 to develop high-fidelity exoatmospheric time-varying RCS models of the objects of six USSR ICBM and SLBM systems at L-band and UHF frequencies. These models have been developed and validated through analysis and comparisons with recorded COBRA DANE and ARIS RCS data on USSR missile system tests. These data are maintained in rapid-access computer files. Currently the L-band RCS data base contains 5629 tracks from 248 COBRA DANE missions covering 21 different missile systems. These L-band data represent a total of over 336 hours of RCS observations. The UHF data base currently includes 473 histories representing approximately 7 hours of ARIS RCS observations covering 15 different missile systems.

Five algorithms were developed by TBE to simulate the sets of observed RCS data characteristics of objects to be modeled. These algorithms utilize discrete inputs from a tunable variable space defined for each modeled object. These tunable parameters were generally specified in terms of probability distributions for each model developed to provide for observed mission-to-mission variations in the recorded RCS data. Section 2 of this report presents a brief description of the time-varying RCS modeling algorithms that were developed. A detailed description of each algorithm is given in the appendices. An identification of the algorithm utilized for each object of the USSR weapon systems that have been modeled is given in Reference 1.

Section 3 provides a discussion of the procedures used for RCS model validation. Part of this procedure consisted of comparing the values of discrimination signatures calculated from the recorded and the model data. A definition of these signatures is provided. The potential effects of random noise on these signatures is also discussed.

2. RCS MODEL ALGORITHMS DEVELOPMENT

During the process of developing time-varying RCS models of the various objects of six USSR ICBM and SLBM weapon systems, various algorithms were developed to simulate the observed RCS time structure and RCS discrimination signatures of the recorded data at L-Band and UHF frequencies. The RCS modeling proceeded concurrently with the TBE development of flight models for the same weapon systems. As objects were identified by the flight modeling efforts, the associated RCS data were analyzed. Differing RCS data structures observed for the different object types has led to the development of several algorithms.

These algorithms were separately documented as they were developed by TBE. These documents have been edited and revised to reflect the current form of the algorithm and are included as Appendices A through E. A brief description of each algorithm is given in the following sections.

2.1 SPB ALGORITHM

The Static Pattern Based (SPB) algorithm has been employed to develop RCS models for large, well defined, roll-symmetric objects (e.g. cylinders, cones, etc) with well defined body motion. This algorithm provides viewing and body motion sensitivities. Observed RCS data for these objects are largely cyclically repetitive as a function of time. An RCS static pattern (RCS in dBsm vs aspect angle) is used in this algorithm to provide an RCS estimate as a function of the aspect angle which is computed from the modeled body motion and the radar viewing parameters at each model simulation time. The RCS static patterns for this algorithm are based upon analytic calculations from intelligence estimates of the object size and shape as well as the observed RCS data. The SPB algorithm is documented in Appendix A.

2.2 MSPB ALGORITHM

The Modified Static Pattern Based (MSPB) algorithm is similar to the SPB algorithm, but also models spin motion for non-roll symmetric objects. This algorithm also supports the modeling of scattering from objects composed of multiple bodies. The MSPB algorithm models both the main body motion and the relative motion of any additional scatterers. The model parameters include motion parameters which are trajectory dependent as well as motion parameters which are trajectory independent. The MSPB algorithm is detailed in Appendix B.

2.3 CORS ALGORITHM

TBE developed the Correlated Statistical (CORS) algorithm for objects whose RCS histories are essentially random in nature. This model does not include any body motion or radar viewing parameters. The CORS algorithm simulates the observed RCS data by computing correlated random draws from a constrained Gaussian distribution in dBsm space. The correlation function is modeled as an exponential time decay. The mathematical description of the CORS algorithm is provided in Appendix C.

2.4 SARP ALGORITHM

The Sinusoids and Random Process (SARP) algorithm was developed to model RCS characteristics that contain significant time structure that cannot be associated with definable object motion characteristics. Spectral analysis of these RCS data show a pronounced contribution from a limited sequence of sinusoids in addition to a broad-band background. The SARP model simulates this observed structure by summing the contribution from a specified number of harmonically related sinusoids (in dBsm space) and a constrained uncorrelated Gaussian background process. The number of sinusoids, their amplitudes and phases are defined from the power spectra of the RCS data. The SARP algorithm and the required model parameters are described in Appendix D.

2.5 SARP2 ALGORITHM

The SARP2 algorithm was developed for one object whose spectral analysis showed only a limited number of non-harmonic frequency components. Functionally, the SARP2 algorithm is nearly identical to the SARP algorithm (Appendix D). The primary difference between SARP and SARP2 is that SARP2 uses explicitly defined sinusoids that are not constrained to be harmonic. Thus the SARP2 algorithm requires the frequency, amplitude and phase to be defined for each sinusoid.

2.6 MSARP ALGORITHM

The Modified Sinusoids and Random Process (MSARP) algorithm was defined for objects whose RCS spectral data possessed many non-harmonically related sinusoids. These objects are more irregular than those modeled by SARP. Since the MSARP algorithm does not explicitly include motion parameters, this algorithm also does not support radar viewing dependencies. The MSARP algorithm is described in Appendix E.

3. RCS MODEL VALIDATION

The time-varying RCS model for an object consists of the specification of the time-varying algorithm and the required probability distributions for the algorithm input parameters. Validation of a model was comprised of two aspects. The initial aspect was accomplished by visual comparisons of the structure of the real and simulated time histories. Recorded RCS time histories and those produced from the model should show similar structure and basic characteristics. A correspondence should be noted in the troughs and peaks with the same approximate periodicity. Rather than a one-to-one correspondence between an RCS history and a model realization, the model realizations should be representatives of the basic characteristics observed in the data of a particular object. The second aspect of model validation was a comparison between selected RCS discrimination signatures calculated from both the recorded data and the time-varying RCS model. The RCS signatures selected for model validation are identified in Section 3.1. The effects of random noise on these signatures are given in Section 3.2.

3.1 RCS DISCRIMINATION SIGNATURES

The selected RCS signatures include the RCS signatures currently employed by the PARCS for characteristic object processing, the signatures used by the PAVE PAWS automatic object classification subfunction and the signatures used by COBRA DANE (except the coefficient of variation). The power discrimination ratio which had been proposed for EPARCS was also selected as well as two RCS signatures previously proposed by TBE.

The calculated RCS discrimination signatures are:

- peak RCS (PRCS)
- average RCS (ARCS)
- maximum absolute pulse to pulse RCS difference (MPD)
- average absolute pulse to pulse difference (APD)
- power discrimination ratio (PDR)
- RCS variance (VRCS)

- scintillation index (SCIN)
- local variance (LVS)
- local residual (LRS)

All signatures except the PDR are calculated in dBsm space. The PDR is calculated in M^2 space. The PDR is essentially the ratio of low frequency content to the total RCS observation. The SCIN can be considered as the ratio of the high frequency to low frequency content. The LVS is the average variance calculated over sets of four RCS observations. The LRS is similar to LVS except the mean square distance is calculated from a least squares straight line fit to the four points. The MPD, APD, LVS, and LRS are calculated only when the time between RCS observations is less than 0.3 seconds. The LVS and LRS require at least 4 consecutive observations meeting this condition. The PDR requires data spaced at a maximum of 1.1 seconds. These selected RCS discrimination signatures, a brief summary of calculation procedures and restrictions are summarized by Table 3-1.

3.2 NOISE EFFECTS ON DISCRIMINATION SIGNATURES

Recognizing the potential for the effects of noise on the signatures calculated from the recorded RCS data, an analysis was performed to illustrate the magnitude of these effects. This analysis consisted of superimposing zero-mean Gaussian random noise constrained to $\pm 3\sigma$ limits on various constant ARCS levels. This process was sampled at a 24 Hz rate for a period of 50 seconds and the RCS signatures were calculated from these 1200 samples. The results of this exercise show that only the ARCS signatures were unaffected by the Gaussian process. Many of the resulting signatures could be approximated from the standard deviation (σ_N) of the simulated Gaussian noise by:

$$\begin{aligned} \text{PRCS} &= \text{ARCS} + 3 \sigma_N \\ \text{MPD} &= 4.8 * \sigma_N \\ \text{APD} &= 1.1 * \sigma_N \\ \text{VRCS} &= \sigma_N^2 \\ \text{LVS} &= 0.72 \sigma_N^2 \\ \text{LRS} &= 0.49 \sigma_N^2 \end{aligned}$$

Corresponding results for the PDR and SCIN signatures are shown by Figures 3-1 and 3-2.

This exercise indicates that any zero-mean Gaussian noise contained in the real RCS data would tend to increase the calculated PRCS, MPD, APD, VRCS, LVS and LRS signatures. The effects on SCIN and PDR are more dependent on the ARCS and the ARCS signature itself is not influenced by zero-mean noise. These effects of noise on the signatures were considered when tuning an RCS model to obtain signatures that correspond to those calculated from the recorded data.

TABLE 3-1. RCS DISCRIMINATION SIGNATURES, PROCEDURES, AND RESTRICTIONS

SYMBOL	SIGNATURE	CALCULATION*	CALCULATION SPACE	RESTRICTION
PRCS	Peak Radar Cross Section	Maximum (RCS_i) $i = 1, N$	dBsm	None
ARCS	Average Radar Cross Section	$\frac{1}{N} \sum_{i=1}^N RCS_i$	dBsm	None
MPD	Maximum Absolute Pulse to Pulse RCS Difference	Maximum $ \Delta RCS_i $ $i = 1, N - 1$	dBsm	$\Delta t \leq 0.3$ sec
APD	Average Absolute Pulse to Pulse RCS Difference	$\frac{1}{N-1} \sum_{i=1}^{N-1} \Delta RCS_i $	dBsm	$\Delta t \leq 0.3$ sec
PDR	Power Discrimination Ratio	$PDR = \frac{Y_2}{S_2}$ $Y_2 = 100 + \sum Y_i^2$ $Y_i = 0.2 * RCS_i + 0.8 * Y_{i-1}$ $Y_0 = 0$ $S_2 = 100 + \sum RCS_i^2$	M ²	$\Delta t \leq 1.1$
VRCS	RCS Variance	$\frac{\sum RCS_i^2}{N} - \left(\frac{\sum RCS_i}{N}\right)^2$	dBsm	None

*N Pulses assumed with N - 1 pulse differences and N/4 four pulse groups.

TABLE 3-1. RCS DISCRIMINATION SIGNATURES, PROCEDURES, AND RESTRICTIONS (concluded)

SYMBOL	SIGNATURE	CALCULATION*	CALCULATION SPACE	RESTRICTION
SCIN	Scintillation Index	$\frac{\text{VRCS} - \text{Variance}(R)}{\text{Variance}(R)}$ $R_i = e^{(-4\pi\Delta t)} R_{i-1}$ $+ (1 - e^{-4\pi\Delta t}) * \text{RCS}_i$ $R_0 = 0$	dBsm	None
LVS	Local Variance	$\frac{1}{N/4} \sum \text{Variance}(\text{RCS}_j) j=1,4$	dBsm	$\left. \begin{array}{l} 4 \\ \text{Consecutive} \\ \text{Pulses} \\ \Delta t \leq 0.3 \end{array} \right\}$
LRS	Local Residual	$\frac{1}{N/4} \sum \text{Mean Square Distance From Least Squares Straight Line}$	dBsm	

*N Pulses assumed with N - 1 pulse differences and N/4 four pulse groups.

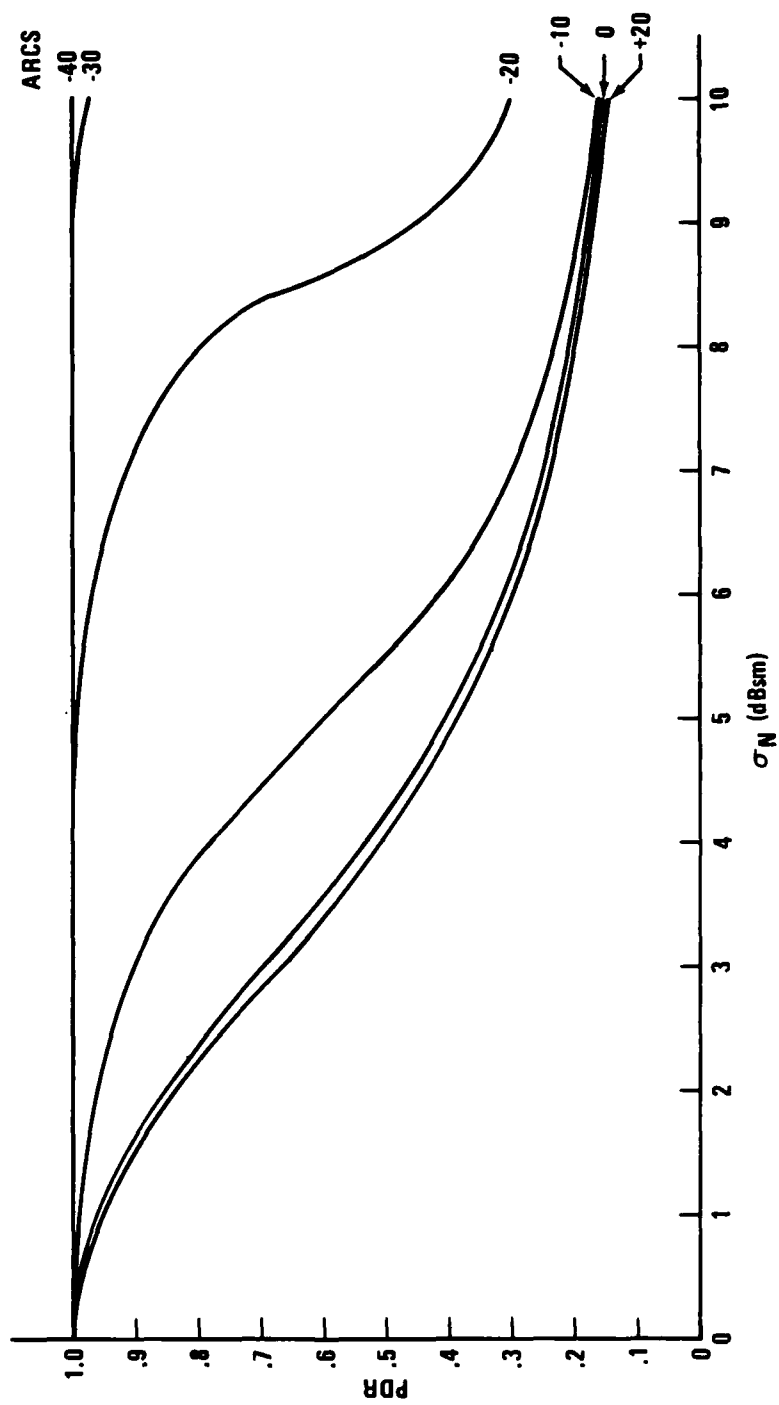


FIGURE 3-1. EFFECTS OF RANDOM NOISE ON PDR WITH CONSTANT ARCS LEVELS

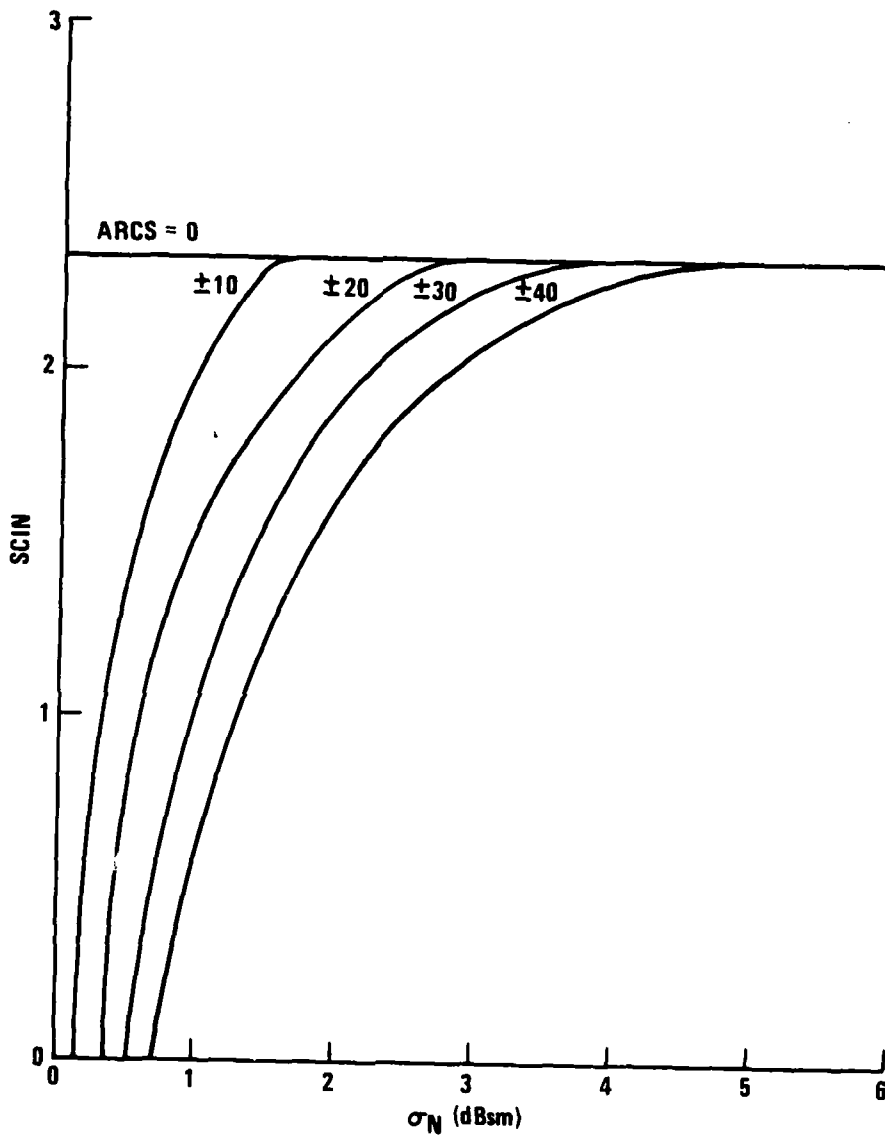


FIGURE 3-2. EFFECTS OF RANDOM NOISE ON SCIN WITH CONSTANT ARCS LEVELS

REFERENCES

1. W. J. Gruner, "Time-Varying RCS Modeling (RCSSMODLER) Program (U)," Teledyne Brown Engineering Technical Report MSB81-WIC-0024, August 1981 (SECRET)

APPENDIX A

STATIC PATTERN BASED (SPB) TIME
VARYING RCS ALGORITHM

By

W. B. Wellman
D. C. Johnson

1. INTRODUCTION

TBE is required to develop exoatmospheric time varying L-band and UHF RCS models for objects of several missile systems under Contract DASG60-79-C-0094. A static pattern based (SPB) time varying RCS generation method is one procedure for simulating RCS histories that have significant time structure. TBE has developed an SPB RCS generation model for this purpose.

Section 2 presents a description of the SPB RCS model. The model parameters including those which define the physical motion characteristics imposed on the object during flight are given. Representative model output for several motion and viewing conditions is presented.

2. STATIC PATTERN BASED RCS GENERATION MODEL

2.1 INTRODUCTION

The RCS scattering characteristics of objects that are roll symmetric, e.g. cylinders, cones, etc., can be represented by a single RCS static pattern for a specified combination of radar transmit and receive polarizations. The static pattern is the RCS amplitude as a function of the viewing angle relative to the body centerline. This angle is called the aspect angle. If the position and orientation of the object relative to the radar at a given transmission time can be determined, the aspect angle at which the radar is viewing the object can be calculated. Then the RCS amplitude from the static pattern at the calculated aspect angle is the RCS for that transmit time. Modeling the body motion as the object flies along its trajectory and computing the aspect angle and then the RCS for each transmission time produces a time varying RCS for an object as viewed from a specified radar location.

Thus for this technique, a model of the object motion must be developed and the equations for computing the aspect angle to the object from a given radar location must be derived. The following sections define the object motion model and viewing geometry relationships between the radar and object orientation. Then in Section 2.5 the model implementation is described and example time varying RCS histories are given in Section 2.6.

2.2 BODY MOTION MODEL

The body motion is defined relative to a body motion axis. The body motion axis is defined as a reference axis extending through the body's center of gravity at the position of the body on its ballistic trajectory path. The orientation is defined by an angle ψ relative to a perpendicular to the trajectory plane and by an angle T from a reference axis in the trajectory plane as shown in Figure 1(a).

In this model two types of body motion are included. First, there is precession motion, which is the fundamental cyclical motion of the body about the motion axis. This motion is assumed to occur with the body centerline moving at an angular rate \dot{A} on the surface of a cone P degrees from the motion axis as shown in Figure 1(b). An object purely tumbling in its trajectory plane would correspond to $\psi = 0$ and $P = 90^\circ$.

The second type of body motion modeled is nutation, which is an additional precession motion of the body about the mean body centerline axis. This motion is defined by a angle N from the mean body centerline and an angular rate \dot{D} as shown in Figure 1(c). There are two constraints on the angles N . First N is restricted to be less than P . Second there is a joint constraint between the allowed value of N and the values of \dot{D} and \dot{A} . N is constrained to be less than the maximum of $[15.6845 - \dot{D}/\dot{A}] \times 0.6588$ and $[51.3543 - \dot{D}/\dot{A}] \times 0.0627$. This latter constraint which was empirically derived, is necessary to prevent unrealistic combination model of these parameters.

2.3 RADAR VIEWING GEOMETRY

For the SPB RCS model, the change in the radar line of sight as the object moves along its trajectory path is modeled in an approximate manner. At an initial time t_0 , e.g., when or before the initial time of the desired RCS interval, the angle θ between the radar line of sight and the perpendicular to the trajectory plane is determined. As shown in Figure 2, the radar line of sight vector is projected into the trajectory plane. For convenience, this is used as the reference axis for the angle T defined in Figure 1(a). The angle ϕ between the radar line of sight and the body motion axis, which will be required in Section 2.4, is also identified in Figure 2.

The change in the viewing angle as the object moves along its trajectory path is modeled by assuming that θ changes at a constant rate $\dot{\theta}$. Thus $\theta(t) = \theta_0 + \dot{\theta}(\Delta t)$, where θ_0 is the viewing angle at time t_0 and $\Delta t = t - t_0$.

2.4 ASPECT ANGLE DETERMINATION

The aspect angle will first be determined relative to the body centerline motion, i.e., the precession, and then this equation will be modified to account for the nutation. From Figure 3, the aspect angle ϵ is $\epsilon(t) = \cos^{-1} (\sin \phi(t) \sin P \cos (\dot{A}\Delta t) + \cos \phi(t) \cos P)$, where ϕ is the angle between the radar line of sight and the body motion axis and $\dot{A}(\Delta t)$ is the angular amount that the body centerline has rotated since time t_0 .

From Figure 4, which includes the nutation motion, the angle from the body motion axis to the body centerline is the angle P plus the change due to the nutation. This approximate change in P due to the nutation is $N \cdot \cos(\dot{D}\Delta t)$. The change in the precession rotation is approximately $\tan^{-1}(\tan N \sin(\dot{D}\Delta t) \sin P)$. Thus, including the nutation, the equation for the aspect angle becomes

$$\begin{aligned} \epsilon(t) = & \cos^{-1} [\sin \phi(t) \sin (P + N \cdot \cos(\dot{D}\Delta t)) \\ & \cdot \cos(\dot{A}\Delta t + \tan^{-1}(\tan N \cdot \sin(\dot{D}\Delta t)/\sin P)) \\ & + \cos \phi(t) \cos (P + N \cdot \cos(\dot{D}\Delta t))] \end{aligned} \quad (1)$$

To complete the computation of $\epsilon(t)$, $\phi(t)$ is required. From Figure 2,

$$\begin{aligned} \phi(t) = & \cos^{-1} [\sin \psi \sin(\theta_0 + \dot{\theta}\Delta t) \sin T \\ & + \cos \psi \cos(\theta_0 + \dot{\theta}\Delta t)] \end{aligned} \quad (2)$$

2.5 MISSION-TO-MISSION VARIABILITY PARAMETERS

Recorded RCS data from objects for which the SPB algorithm was used have shown an unexplained variability in the peak RCS from mission to mission. To model this variation a small amplitude slowly varying sinusoid, $A_s \sin(2\pi T/T_s)$, is added to the computed RCS values. These two parameters, A_s and T_s , given in Table 3, complete the parameter definition of the model. The variable T is the sum of the relative simulation time and an initial uniform random draw from the interval $(0, T_s)$.

2.6 MODEL IMPLEMENTATION

From the preceding sections, six motion and two mission-to-mission variability parameters for the model have been defined. These are given in Tables 1 and 3. The use of this model requires a definition of each parameter. In general, these definitions will be in the form of probability density functions to account for the variability in object motion that is typically observed on various test flights of the same object.

To complete the SPB RCS model, the static pattern is required. This can be either an analytical expression or a table of RCS amplitude as a function of the aspect angle. In the latter case, the RCS is obtained by linear interpolation.

The use of this model requires the definition of the radar viewing condition parameters given in Table 2. The value of θ_0 can be approximated or calculated from the relationship between the radar and the object on its ballistic trajectory at time t_0 .

After the model and radar viewing parameters have been established for t_0 , the use of the equations (1) and (2) with $\Delta t = t - t_0$ provides the value of ϵ at time t . The RCS at time t is determined for the calculated value of ϵ .

2.7 SPB RCS MODEL EXAMPLES

Figure 5 shows an analytical static pattern of RCS amplitude in dBsm as a function of aspect angle in degrees. The pattern was generated from $RCS = (\sin x/x)^2$, where $x = 10.1664 \cos \Omega$.

Figure 6 and 7 show examples of the SPB RCS model output using the static RCS pattern in Figure 5 and with a 10-Hz sample rate. Figure 6 shows the effect of changes in the radar location and precession motion on the time varying RCS history. Figure 7 shows the effects of nutation motion with the radar in the trajectory plane and the object tumbling in the plane of the trajectory. The effects of precession motion and radar

location changes result in varying the region of the static RCS pattern within which sampling takes place. The addition of nutation motion results in increased scintillation in the time varying RCS. In Figure 6 and 7, A_s and $\dot{\theta}$ set to zero because the time intervals were too short to notice an appreciable effect on the time varying RCS due to trajectory and radar viewing geometry changing with time.

TABLE 1. SPB RCS MODEL MOTION PARAMETERS

SYMBOL	DESCRIPTION
ψ	Angle between body motion axis and perpendicular to trajectory plane (Deg)
T	Angle in trajectory plane between projection of body motion axis and radar line of sight at time t_0 (Deg)
P	Precession Angle (Deg)
$T_P = \frac{360}{\dot{A}}$	Precession Period (sec)
N	Nutation Angle (Deg)
\dot{D}	Nutation Angular Rate (Deg/sec)

TABLE 2. RADAR VIEWING CONDITION INPUT FOR SPB RCS MODEL

SYMBOL	DESCRIPTION
θ_0	Angle between radar line of sight and perpendicular to trajectory plane at time t_0 (Deg)
$\dot{\theta}$	Angular rate of change of θ (Deg/sec)

TABLE 3. SPB RCS MODEL MISSION-TO-MISSION
VARIABILITY PARAMETERS

SYMBOL	DESCRIPTION
A_s	Sinusoid Amplitude (dBsm)
T_s	Sinusoid Period (sec)

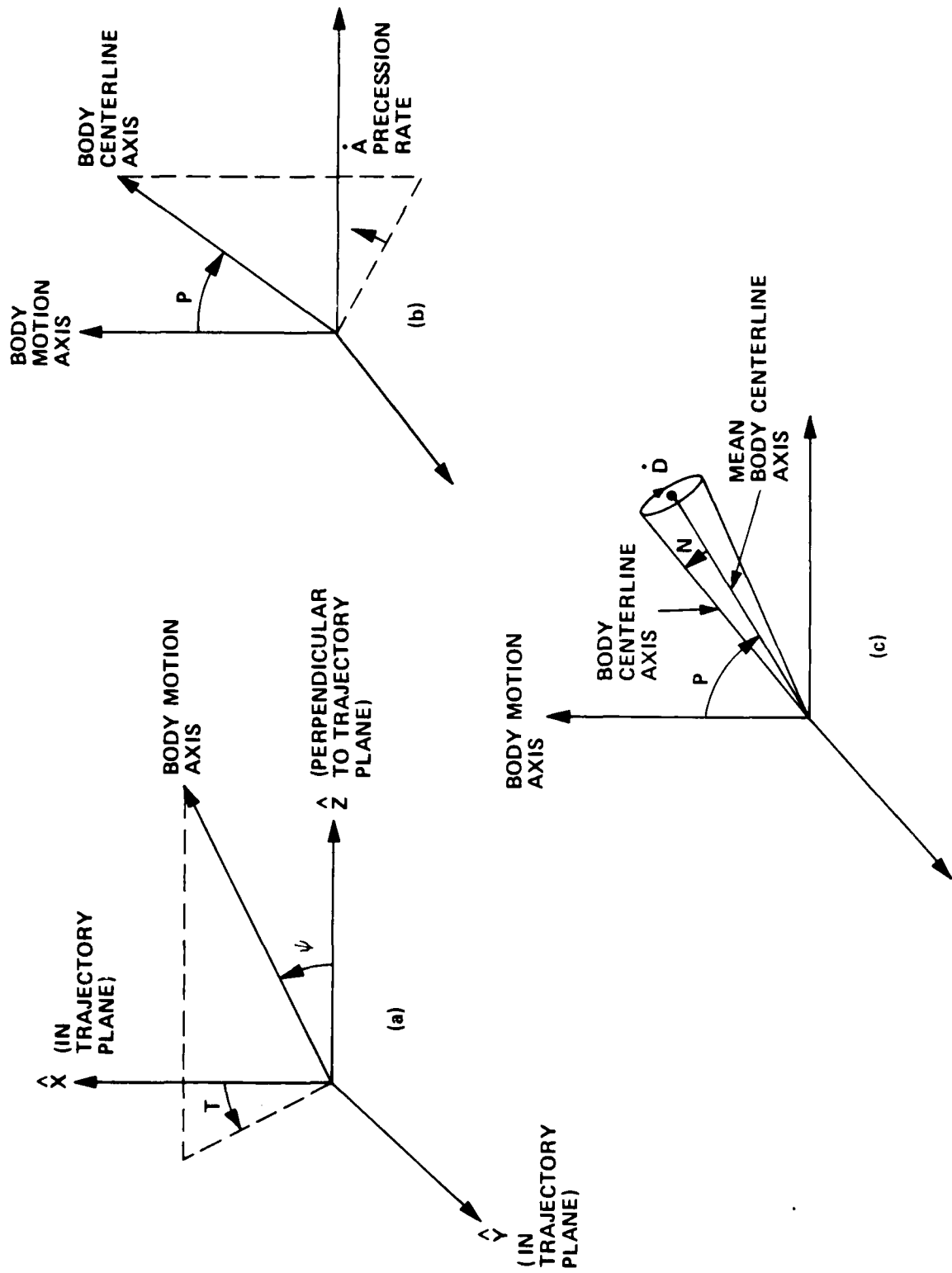


FIGURE 1. BODY MOTION MODEL

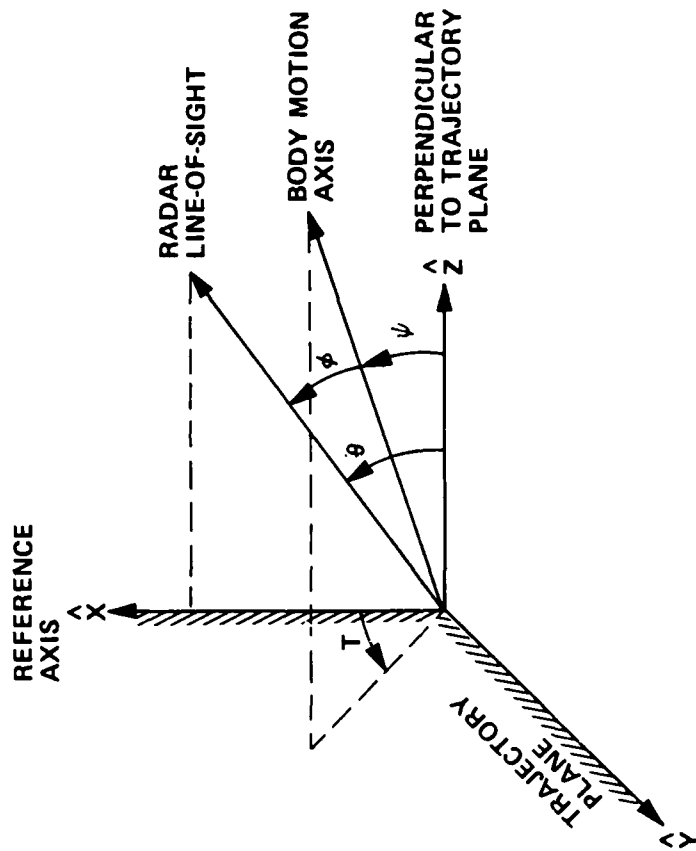


FIGURE 2. RADAR, TRAJECTORY, AND BODY MOTION AXIS GEOMETRY

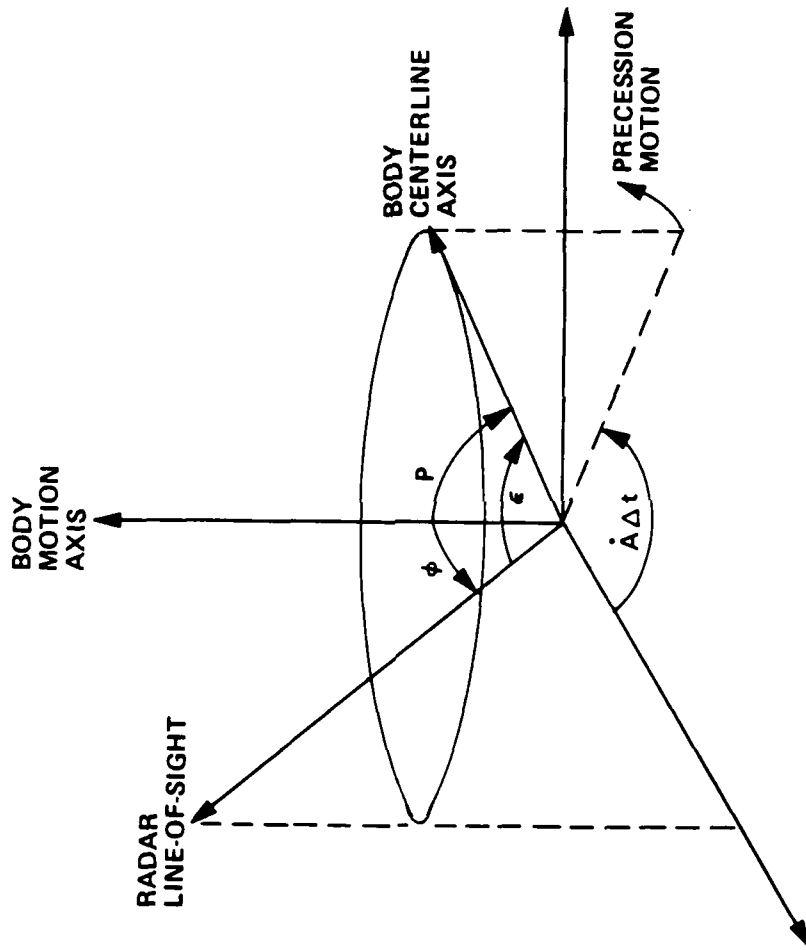


FIGURE 3. BODY PRECESSION MOTION GEOMETRY

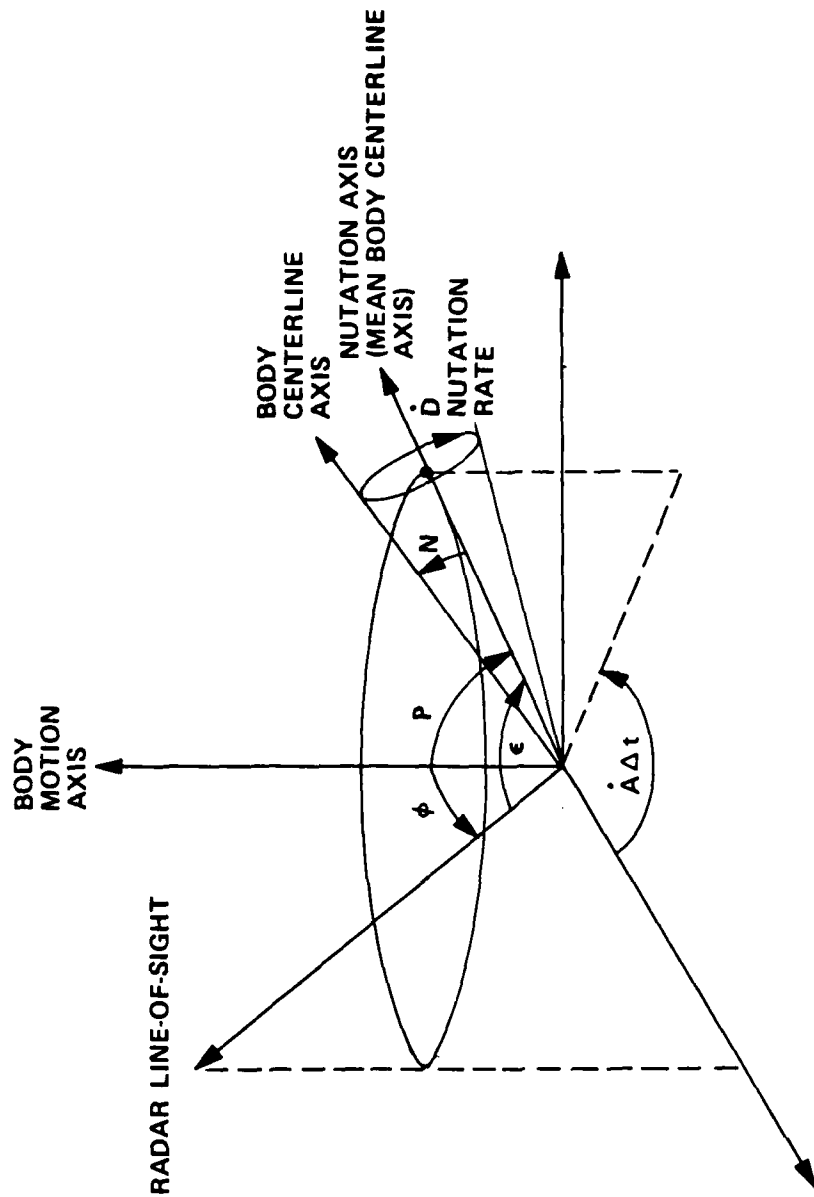


FIGURE 4. BODY NUTATION MOTION GEOMETRY

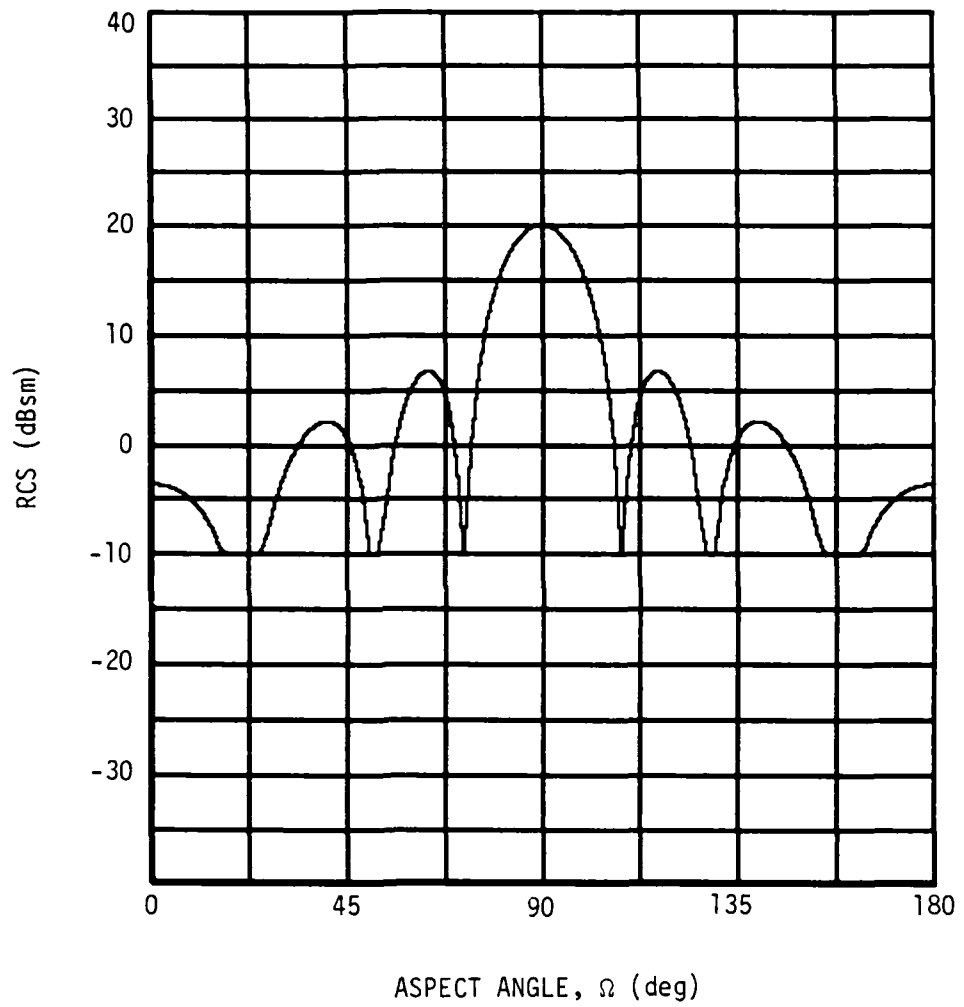
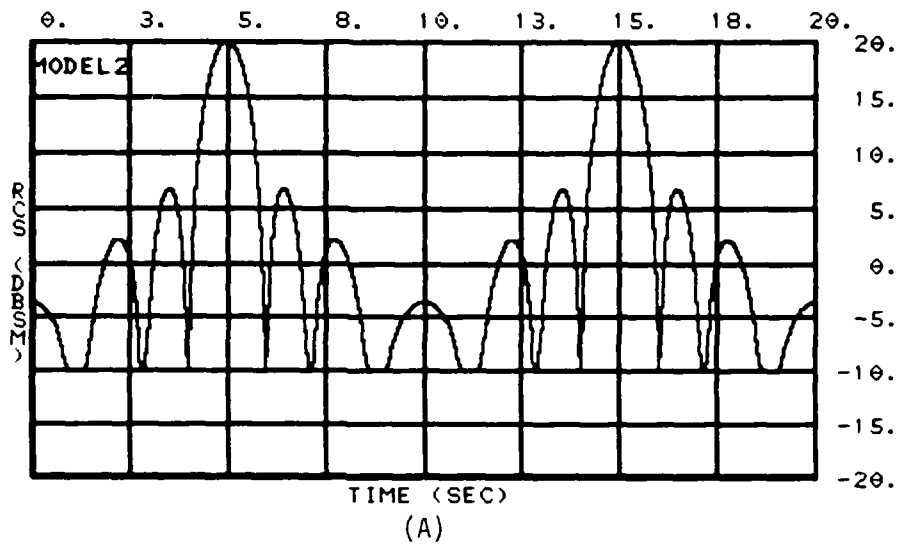
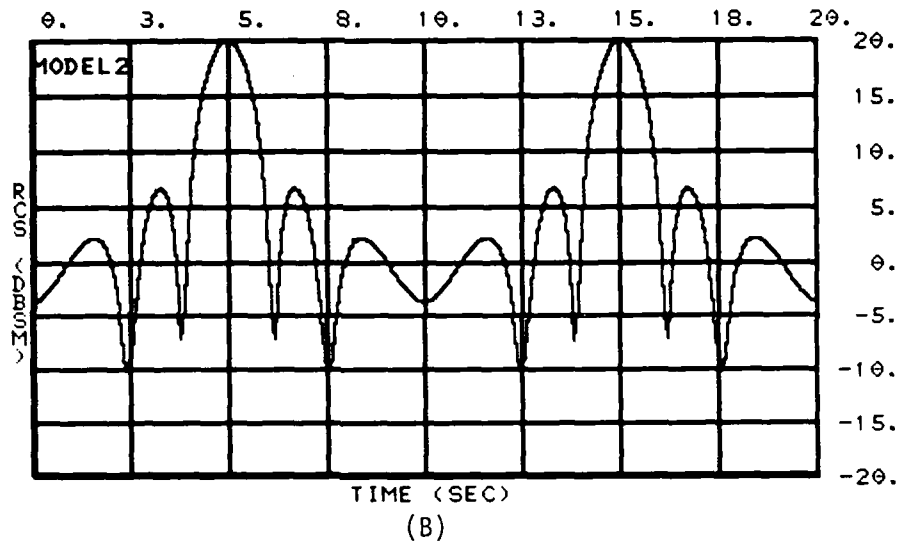


FIGURE 5. HYPOTHETICAL STATIC PATTERN

$\psi = 0 \text{ deg}$
 $T = 0 \text{ deg}$
 $P = 90 \text{ deg}$
 $\dot{A} = 18 \text{ deg/sec}$
 $N = 0 \text{ deg}$
 $\dot{D} = 0 \text{ deg/sec}$
 $\theta = 90 \text{ deg}$



$\psi = 10 \text{ deg}$
 $T = 180 \text{ deg}$
 $P = 90 \text{ deg}$
 $\dot{A} = 18 \text{ deg/sec}$
 $N = 0 \text{ deg}$
 $\dot{D} = 0 \text{ deg/sec}$
 $\theta = 50 \text{ deg}$



$\psi = 20 \text{ deg}$
 $T = 0 \text{ deg}$
 $P = 60 \text{ deg}$
 $\dot{A} = 18 \text{ deg/sec}$
 $N = 0 \text{ deg}$
 $\dot{D} = 0 \text{ deg/sec}$
 $\theta = 80 \text{ deg}$

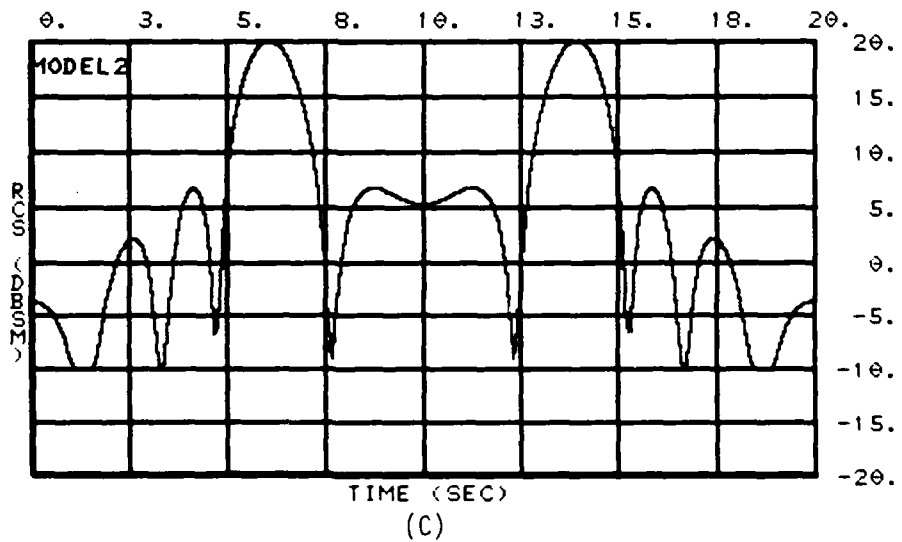
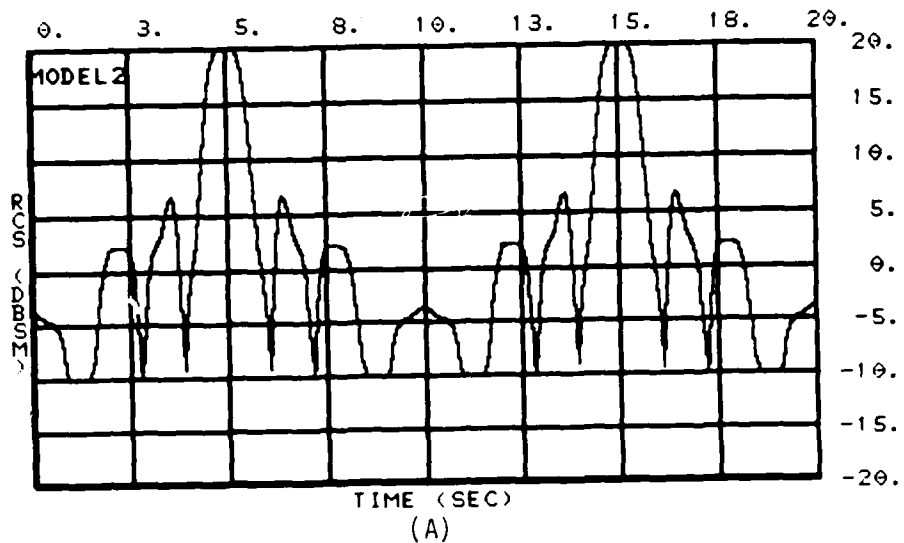
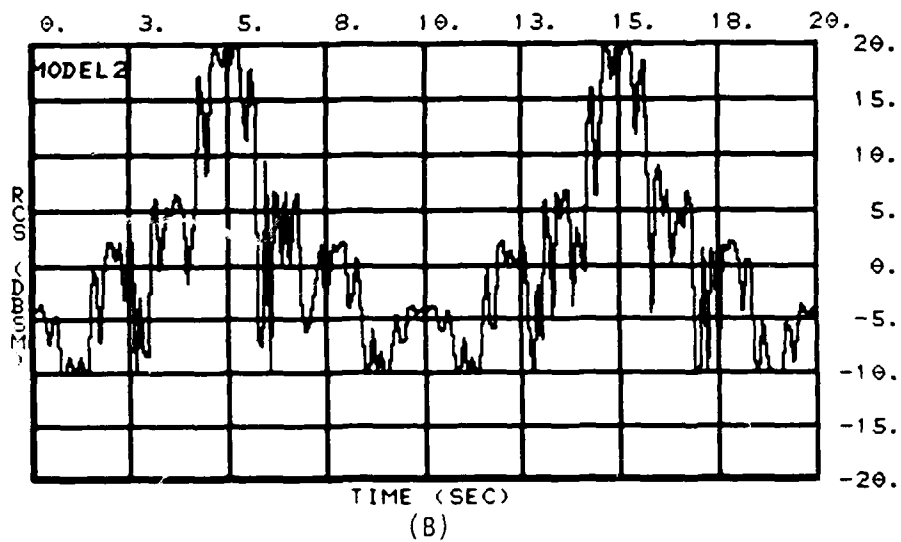


FIGURE 6. SPB RCS TIME VARYING MODEL

$\psi = 0 \text{ deg}$
 $T = 0 \text{ deg}$
 $P = 90 \text{ deg}$
 $A = 18 \text{ deg/sec}$
 $N = 2 \text{ deg}$
 $D = 396 \text{ deg/sec}$
 $\theta = 90 \text{ deg}$



$\psi = 0 \text{ deg}$
 $T = 0 \text{ deg}$
 $P = 90 \text{ deg}$
 $A = 18 \text{ deg/sec}$
 $N = 5 \text{ deg}$
 $D = 941 \text{ deg/sec}$
 $\theta = 90 \text{ deg}$



$\psi = 0 \text{ deg}$
 $T = 0 \text{ deg}$
 $P = 90 \text{ deg}$
 $A = 18 \text{ deg/sec}$
 $N = 15 \text{ deg}$
 $D = 1852 \text{ deg/sec}$
 $\theta = 90 \text{ deg}$

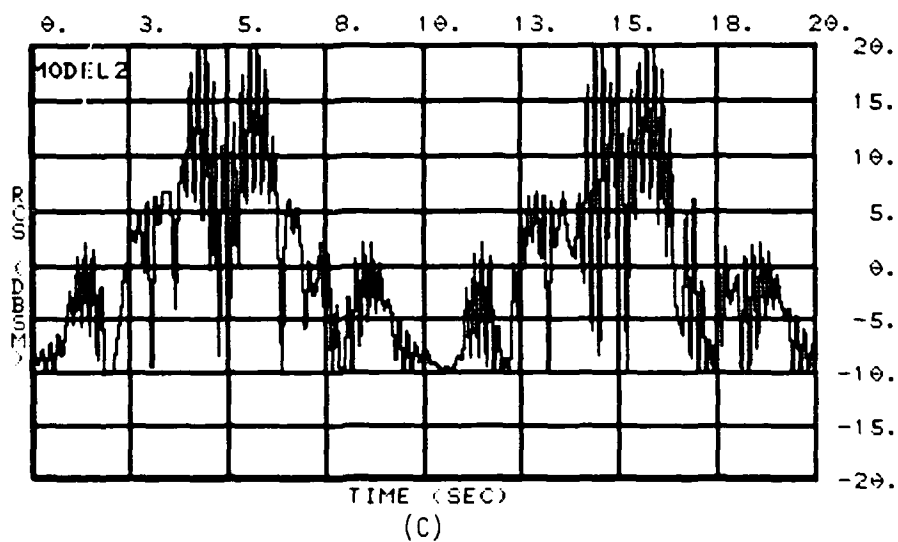


FIGURE 7. SPB RCS TIME VARYING MODEL

APPENDIX B

MODIFIED STATIC PATTERN BASED (MSPB)
TIME VARYING RCS ALGORITHM

By
J. R. Yanosky

1. INTRODUCTION

Teledyne Brown Engineering (TBE) is required to develop exo-atmospheric time varying L-band and UHF radar cross section models for objects of several missile systems under Contract DASG60-79-C-0094. One relevant class of objects requires a particular spatial orientation during flight and is not in general roll-symmetric. TBE has developed a modified static-pattern-based (MSPB) RCS generation method for modeling such objects. Section 2 of this report describes the general nature of the objects being considered and the relative motions such objects are likely to possess. The object and object motion parameters are trajectory independent variables. The spatial orientation of the object and the relationship of this orientation to the motion of the object is detailed in Section 3. The parameters associated with the particular spatial orientation required by the object during flight are trajectory dependent variables. Section 4 outlines the method used to tie the radar location to the spatial orientation of the object. The parameters necessary to affect this characterization are viewing dependent variables. Section 5 then presents a summary which describes the method by which all the parameters are brought together to form a time-varying RCS model. Finally, Section 6 presents an example implementation of the model. Much of the mathematics used in this model is detailed in Appendix A, and references to equations from the appendix are prefixed with an A.

2. TRAJECTORY INDEPENDENT VARIABLES

2.1 OBJECT DEFINITION (BODY COORDINATE SYSTEM)

When the dimensions of the object in terms of the viewing radar wavelength are large, the general technique for estimating the object's RCS consists of establishing a model in which the RCS is due to a number of component scatterers. Once a model has been established for the various component scatterers, the relative magnitudes of the scattered fields from these components are determined, and their contributions are then added with the proper phase to provide an estimate of the RCS of the entire object. Such a procedure must be carried out for all possible, non-redundant aspect angles to obtain a complete RCS static pattern for the object. In the case of roll-symmetric objects, the symmetry permits tabulation of complete RCS information in a relatively short listing. Such symmetry is made use of in TBE's static pattern based, time varying RCS generation model described in Appendix A. The fact that all objects are not roll-symmetric has necessitated the development of the MSPB model.

Figure 1 represents an asymmetric object with a number of scattering components which are fixed in a body coordinate system. The origin of the coordinate system is located at the center of gravity of the object, and the scattering component most closely associated with the origin is termed the primary scatterer. The vector location of the i^{th} scattering component and its RCS contribution are designated \vec{S}_i and σ_i , respectively. The accuracy of the MSPB model improves as the magnitude of each \vec{S}_i gets larger relative to the radar wavelength. Also note that each scattering component may or may not be physically connected to other scatterers and in fact may move about in some random or deterministic fashion in the body coordinate system. That is, \vec{S}_i may be a function of time.

The vector which points to the viewing radar location from the origin of the body coordinate system is the $\hat{L}\hat{O}\hat{S}$ vector. As shown in Figure 2, this vector forms a polar angle θ_L and an azimuth angle ϕ_L

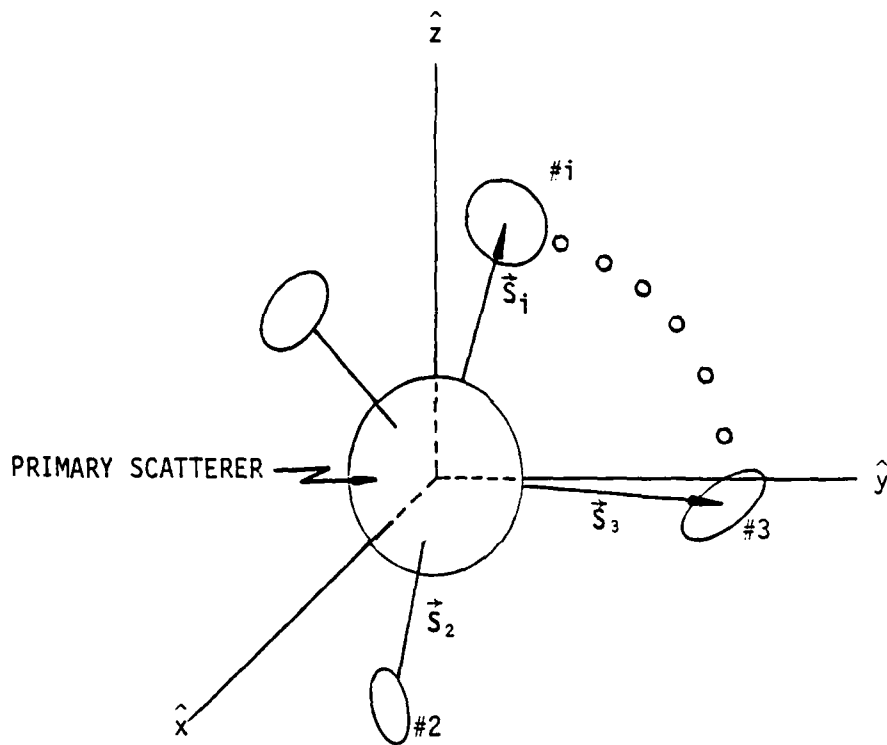


FIGURE 1. BODY COORDINATE SYSTEM SHOWING THE POSITIONS OF THE VARIOUS SCATTERING CENTERS OF THE OBJECT

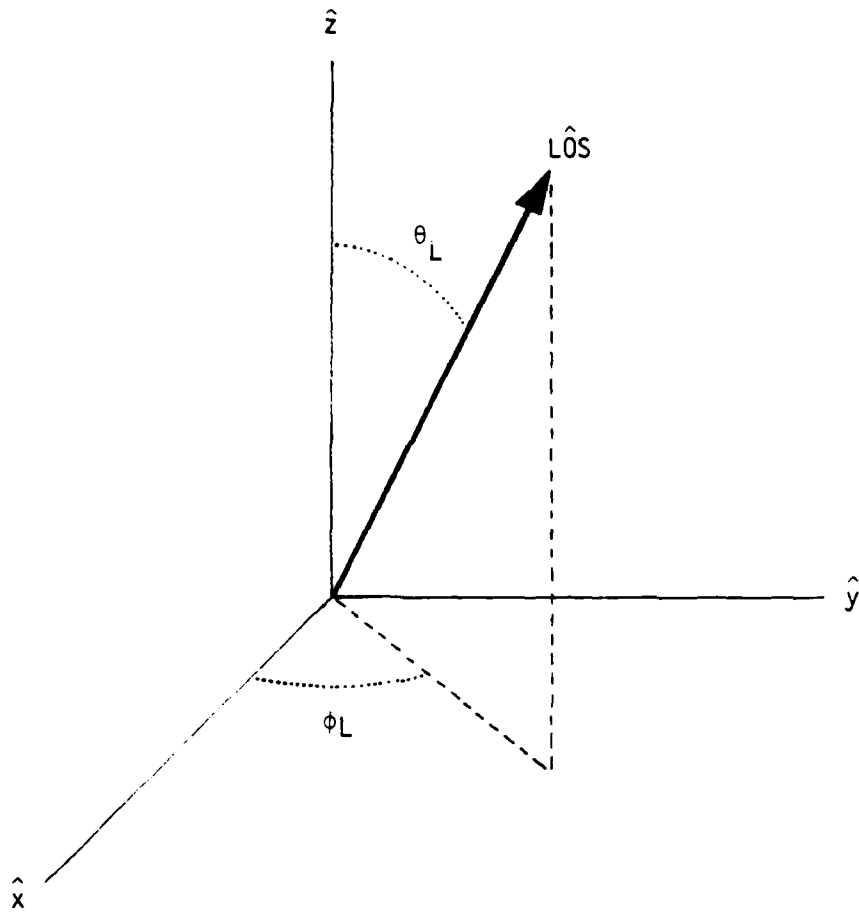


FIGURE 2. LOS VECTOR IN THE FIXED BODY COORDINATE SYSTEM

in the body coordinate system, and the RCS contribution from each scattering component is a function of either one or both of these angles. Namely,

$$\sigma_i = f_i(\theta_L, \phi_L). \quad (1)$$

The form of the function depends on the scattering component and may range from a static pattern look-up table or a simple algorithm to some very involved analytic expression which is being used to estimate the RCS of the complex shape.

The proper phase of each scattering component (ϕ_i) is obtained by referencing the phase to the origin of the coordinate system and adding the phase delay (Δ_i) of each scatterer to that value. That is:

$$\phi_i = k \vec{S}_i \cdot \hat{LOS} + \Delta_i \quad (2)$$

where $k = 2\pi/\lambda$ is the wave number. The estimated RCS of an object with M scattering components is given by:

$$RCS = \left| \sum_{i=1}^M \sqrt{\sigma_i} e^{j2\phi_i} \right|^2. \quad (3)$$

The RCS value calculated in Equation (3) will vary with time because of changing values of θ_L and ϕ_L . These angles vary because the object both flies along a trajectory and moves about its center of gravity.

2.2 OBJECT MOTION (MOTION AXIS COORDINATE SYSTEM)

The motion of a rigid body in the absence of external torques can be specified by three independent parameters called the Eulerian angles (α, β, γ). The angular momentum vector of this rigid body is constant and so has a fixed direction in space which in this report is called the motion axis (MA). Spin is a periodic rotation of a rigid body about its own centerline. However, as the body spins, an observer fixed in the body coordinate system will see a rotation of the spin

angular velocity vector about the motion axis. This second rotation is called precession. The angle between the body centerline and the motion axis is called the coning angle and is itself subject to a periodic change called nutation.

During that portion of an object's trajectory which is exoatmospheric, the object is subject to no external torques, and, therefore, its motion can be specified by the Eulerian angles α , β , and γ as shown in Figure 3. For this to be true, however, the angular velocity vector direction of the object had to have been chosen as the \hat{z} -axis for the body coordinate system. This axis is usually the object's centerline.

Movement of the object about the motion axis is simulated by describing the angles α , β , and γ as functions of time. This movement is referenced to the motion axis coordinate system which has axes (\hat{a} , \hat{b} , \hat{MA}). The directions of the \hat{a} - and \hat{b} -axes will be specified in Section 3. To initialize the angles α , β , and γ in the motion axis coordinate system, assume that at the beginning of the history ($t = 0$):

$$\begin{aligned}\alpha(0) &= \alpha_0 \\ \beta(0) &= \beta_0 \\ \gamma(0) &= \gamma_0.\end{aligned}\tag{4}$$

The rate of change of $\beta(t)$ determines the precession of the object about the motion axis as shown in Figure 3. If the precession period is T_p , then the value of β at any time t is given by:

$$\beta(t) = \beta_0 + \frac{2\pi t}{T_p}.\tag{5}$$

The value of γ at the same time t is somewhat more complicated.

It is a property of the Eulerian angles that movement of the line of nodes (see Figure 3) in the \hat{a} - \hat{b} plane imparts an apparent spin on the object in inertial space. More simply, as the object with no spin precesses about the motion axis, it keeps its same side toward that axis. To obtain the desired inertial spin period (T_s), γ must be calculated using Equation 6.

$$\gamma(t) = \gamma_0 + 2\pi\left(\frac{1}{T_s} - \frac{1}{T_p}\right)t \quad (6)$$

If nutation is expected, the angle $\alpha(t)$ is given by:

$$\alpha(t) = \alpha_0 + A_N \sin \left[\frac{2\pi t}{T_N} \right] \quad (7)$$

where A_N is the nutation amplitude and T_N is the nutation period.

The Eulerian angles are all that is necessary to relate the body coordinate system to the motion axis coordinate system. A vector which has a known direction in either coordinate system can be transformed into the other coordinate system using the \underline{D} -matrix defined in Equation (A7). In Section 2.1, it was shown that a total RCS could be calculated if the direction of the line-of-sight to the radar were known. If the $\hat{L}\hat{O}\hat{S}$ vector is known in the motion axis system, its transformation into the body system using the \underline{D} -matrix and Equations (5) and (6) will lead to a simulation of object motion which can include spin, precession, and nutation.

3. TRAJECTORY DEPENDENT VARIABLES

3.1 PRINCIPLE AXIS COORDINATE SYSTEM

A number of objects for which models are required are oriented relative to a particular spatial direction called the principle axis (\hat{P}_A). This axis, which lies in the trajectory plane, can be specified by the user or by flight models which have been developed by TBE. Figure 4 shows the coordinate system which has been constructed about the principle axis and the flight trajectory plane.

The trajectory plane of an exoatmospheric ballistic object is formed by the intersection of that object's instantaneous velocity vector and a vector (gravity) which points to the center of the earth. In an inertial frame of reference, the trajectory plane remains unchanged during flight because the only force acting on an exoatmospheric ballistic object is gravity. Since the trajectory plane is inertially stable, its perpendicular is ideally suited for an inertially fixed coordinate system.

To form the principle axis coordinate system, the trajectory plane perpendicular (\hat{L}) and the principle axis (\hat{P}_A) are chosen as the first and third axes, respectively. The positive sense of \hat{P}_A is such that the vector to the center of the earth has a positive component along the \hat{P}_A -axis, and the trajectory plane perpendicular is chosen so that the second axis (\hat{v}) has a positive velocity component. Therefore,

$$\hat{v} = \hat{P}_A \times \hat{L} .$$

The principle axis coordinate system is now uniquely defined at the time the principle axis is chosen and is invariant during the exoatmospheric portion of the flight.

3.2 MOTION AXIS

The relationship between the motion axis and the principle axis is shown in Figure 5. When the object is deployed during its flight, its motion axis points in a particular direction relative to the principle

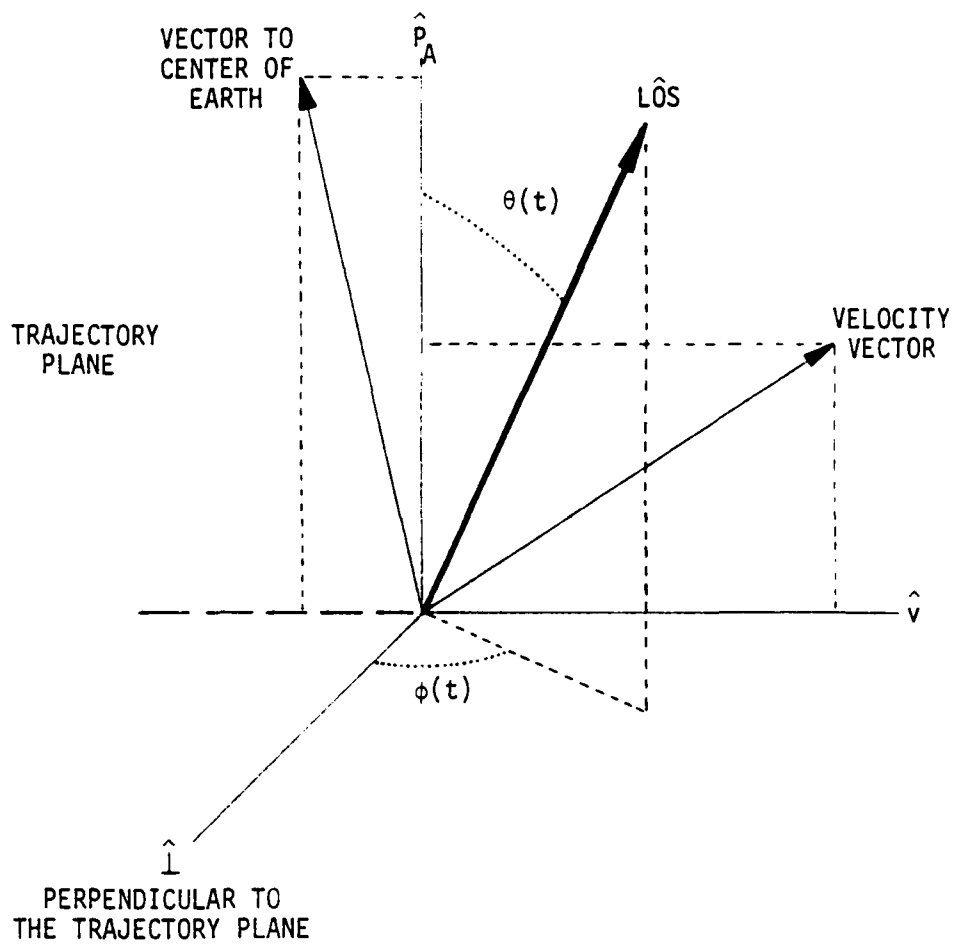


FIGURE 4. THE PRINCIPLE AXIS COORDINATE SYSTEM AND THE RADAR LINE OF SIGHT (LOS)

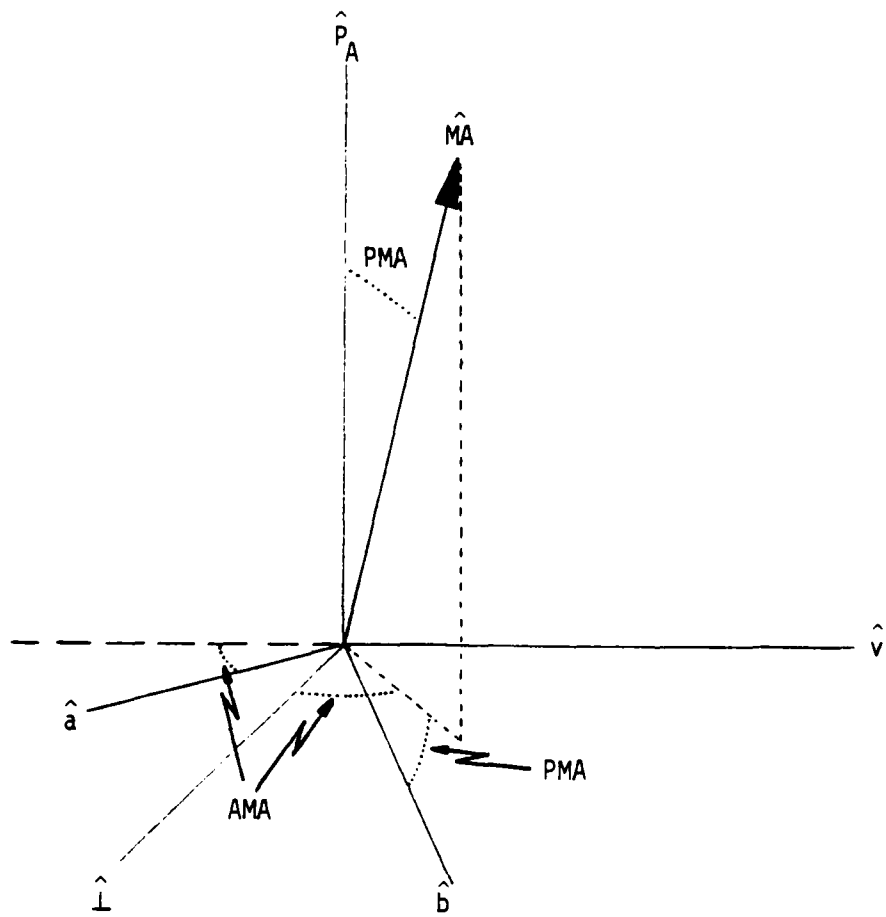


FIGURE 5. MOTION AXIS (\hat{MA}) OF THE OBJECT IN THE PRINCIPLE AXIS COORDINATE SYSTEM

axis. The angle between the \hat{P}_A -axis and the $\hat{M}A$ -axis is called PMA (motion axis polar angle). The angle between the trajectory plane perpendicular and the projection of the motion axis in the $\hat{I}-\hat{V}$ plane is called AMA (motion axis azimuth angle).

A new coordinate system -- the motion axis coordinate system -- is now defined with $\hat{M}A$ as its third axis and \hat{a} and \hat{b} as its first and second axes, respectively, as shown in Figure 5. The transformation matrix from the principle axis coordinate system to the motion axis coordinate system is defined by the \underline{A} -matrix described in the appendix. The directions \hat{a} and \hat{b} are uniquely defined by the transformation in Equation (A5). If the object is deployed so that the $\hat{M}A$ -axis aligns exactly with the principle axis, the \underline{A} -matrix becomes the identity matrix.

It was stated in Section 2.2 that if the $\hat{L}OS$ -vector were known in the motion axis coordinate system, an RCS calculation could be made. Continuing the logic, if the $\hat{L}OS$ vector is known in the principle axis coordinate system, it can be transformed into the motion axis system using the \underline{A} -matrix defined by Equation (A5). The characterization of the $\hat{L}OS$ vector in the principle axis coordinate system is discussed in the following section.

4. VIEWING DEPENDENT VARIABLES

As the object moves along its flight path, the direction of the vector from the center-of-gravity (origin of the principle axis coordinate system) to the radar location ($\hat{L}\hat{O}\hat{S}$) changes -- see Figure 4. Thus, in the principle axis system, $\theta(t)$ and $\phi(t)$ are functions of time. The time history of these two angles defines the inertial direction of the principle axis, characterizes the flight trajectory and the trajectory plane, and pinpoints the radar location. The TBE developed flight models can be used to generate $\theta(t)$ and $\phi(t)$ for any trajectory, principle axis, and radar location for use in the MSPB motion generator. These calculations can be made in real time during a simulation, but time can be saved using other techniques.

If the viewing parameters are such that the angle functions $\theta(t)$ and $\phi(t)$ are reasonably smooth, these angles can be approximated by an N^{th} power polynomial in time. Essentially:

$$\theta(t) = \sum_{n=0}^{N_{\theta}} A_n t^n \quad (8)$$

$$\phi(t) = \sum_{n=0}^{N_{\phi}} B_n t^n. \quad (9)$$

Should they not be smooth, the angles can be listed in a look-up table as a function of time. In either case, a real time simulation can be implemented.

Once $\theta(t)$ and $\phi(t)$ are known at a given moment, the $\hat{L}\hat{O}\hat{S}$ -vector in the principle axis coordinate system is given by:

$$\hat{L}\hat{O}\hat{S} \left(\hat{\perp}, \hat{v}, \hat{P}_A \right) = \hat{\perp} \sin \theta \cos \phi + \hat{v} \sin \theta \sin \phi + \hat{\perp} \cos \theta. \quad (10)$$

5. SUMMARY

In essence, all motion is relative to the principle axis coordinate system which does not move. As the object, properly oriented, flies along its chosen trajectory, the apparent motion of the viewing radar is modeled by Equations (8), (9), and (10). The viewing dependent parameters are listed in Table 1. The time history of the line-of-sight motion in the principle axis system is the first step in the modeling which is aspect dependent.

Since the motion axis coordinate system is not generally aligned with the principle axis coordinate system -- namely the angular momentum vector of the object is not colinear with the principle axis -- a transformation between the two coordinate systems is necessary. That transformation is Equation (A5) and is used to transform the $\hat{L}\hat{O}\hat{S}$ -vector into the motion axis system.

$$\hat{L}\hat{O}\hat{S}(\hat{a}, \hat{b}, \hat{M}\hat{A}) = \hat{A} \cdot \hat{L}\hat{O}\hat{S}(\hat{l}, \hat{v}, \hat{P}_A) \quad (11)$$

The parameters, called trajectory dependent variables, associated with this transformation are listed in Table 2. The range of values of these variables depends on the object being modeled and somewhat on the trajectory along which the object is moving.

Object spin, precession, and nutation are simulated in the transformation from the motion axis coordinate system to the body coordinate system as defined in Equation (A7). These parameters, which are listed in Table 3, are essentially functions only of the object being modeled, and their ranges cannot be set without knowing something of that object. Additional parameters may become necessary which will complete the model. The $\hat{L}\hat{O}\hat{S}$ -vector in the body system is then

$$\hat{L}\hat{O}\hat{S}(\hat{x}, \hat{y}, \hat{z}) = \hat{D} \cdot \hat{L}\hat{O}\hat{S}(\hat{a}, \hat{b}, \hat{M}\hat{A}) \quad (12)$$

Substituting Equation (11) into (12) yields the final equation for modeling the motion of an object flying along its trajectory.

TABLE 1. MSPB VIEWING DEPENDENT VARIABLES*

SYMBOL	DESCRIPTION
A_n $n=0, 1, 3 \dots$ B_n $n=0, 1, 3 \dots$	Coefficients of the polynomials describing the movement of the line-of-sight in the principle axis coordinate system

* The angles $\theta(t)$ and $\phi(t)$ could also be calculated directly from a trajectory.

TABLE 2. MSPB TRAJECTORY DEPENDENT VARIABLES

SYMBOL	DESCRIPTION
\hat{p}_A	The direction of the principle axis
PMA	Angle between the principle axis and the motion axis (radians)
AMA	Angle between the trajectory plane perpendicular and the projection of the motion axis into the $\hat{1}-\hat{v}$ plane (radians)

TABLE 3. MSPB TRAJECTORY INDEPENDENT VARIABLES

SYMBOL	DESCRIPTION
$\alpha_0, \beta_0, \gamma_0$	Initial coning, precession, and spin angles (radians)
T_p	Precession period (seconds)
T_s	Spin period (seconds)
T_N	Nutation period (seconds)
A_N	Nutation amplitude (radians)

$$\hat{L}OS (\hat{x}, \hat{y}, \hat{z}) = \hat{D} \cdot \hat{A} \cdot \hat{L}OS (\hat{L}, \hat{v}, \hat{P}_A) \quad (13)$$

In essence, Equation (13) represents the motion of the viewing radar as seen by the object. Equations (A11), (A12), and (A13) can be used to generate the angles which are used in Equations (1), (2), and (3) to calculate an RCS for time t .

6. EXAMPLE IMPLEMENTATION

MSPB motion parameters have been defined in the preceding sections. These are listed in Tables 1, 2, and 3. The use of the MSPB generator requires a definition of each parameter. In general, these definitions will be in the form of probability density functions to account for the variability in object motion that is typically observed on various test flights of the same object.

To complete the MSPB model, the RCS (σ_i) and position (S_i) of each scattering components is required. As an example, consider an object with two components:

$$\sigma_1 = 16 \left| \frac{\sin x}{x} \right|^2, \quad x = 23 \sin \theta_L \quad (14)$$

$$\sigma_2 = 16 \left| \frac{\sin Y}{Y} \right|^2, \quad Y = 8 \cos \phi_L \quad (15)$$

$$\vec{S}_1 = \frac{\lambda}{\pi} \hat{x} \quad (18)$$

$$\vec{S}_2 = 0. \quad (18)$$

Scatterer #1 has an RCS which is symmetric about the \hat{z} -axis and is not located at the center of motion but rather some distance along the positive \hat{x} -axis. Scatterer #2 is located at the center of motion but is not symmetric about the \hat{z} -axis. The RCS static patterns of these two scattering components are shown in Figures 6 and 7. Assume that the phase delay (Δ_i) is zero for each component.

Figures 8 through 11 show examples of the MSPB time varying RCS output using the scatterers described above in 40-second histories sampled at a 24 Hz data rate. The MSPB parameters are shown in Table 4. Figure 8 shows the effect of precession only while Figure 9 is the result of spin only. Both figures show the effect of moving along the flight

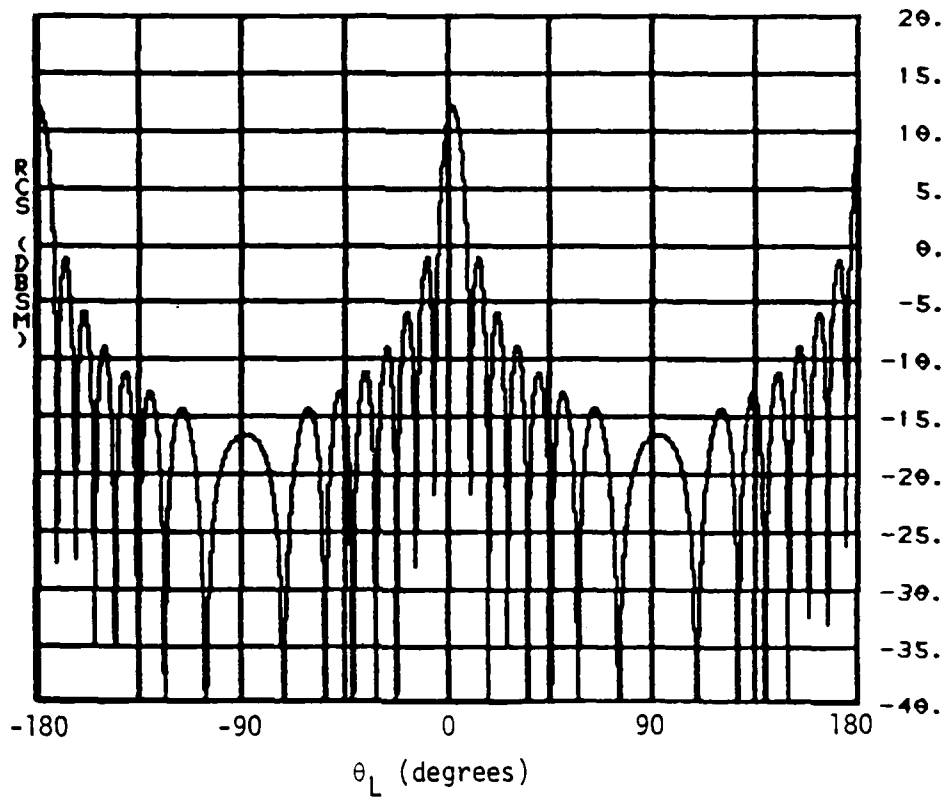


FIGURE 6. RCS STATIC PATTERN OF SCATTERER #1

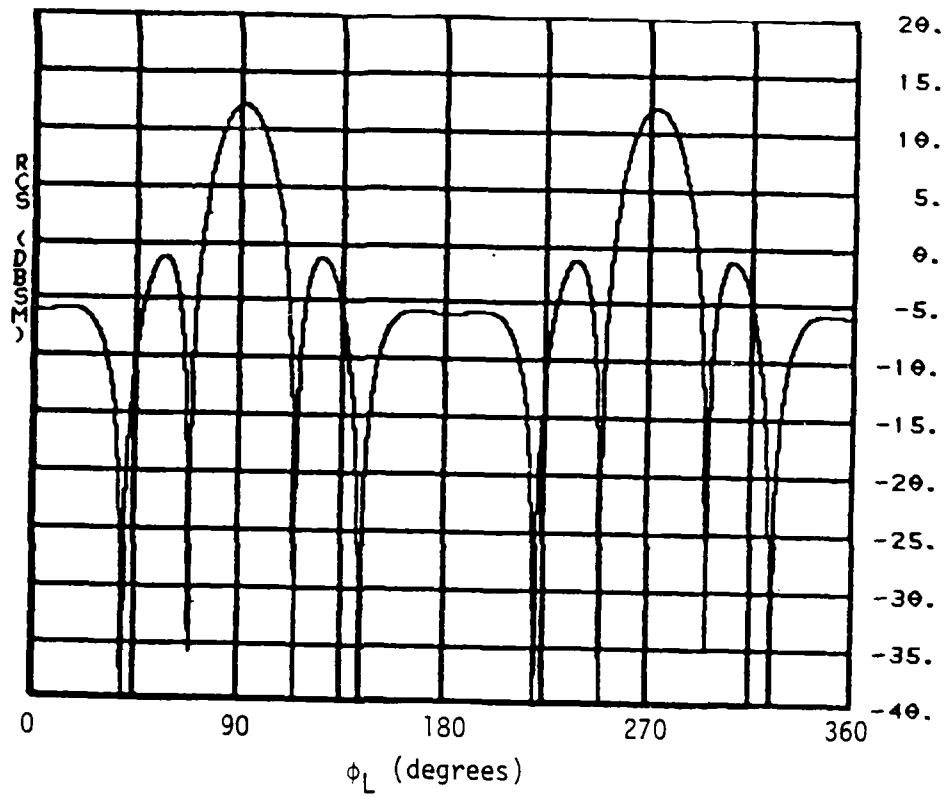


FIGURE 7. RCS STATIC PATTERN OF SCATTERER #2

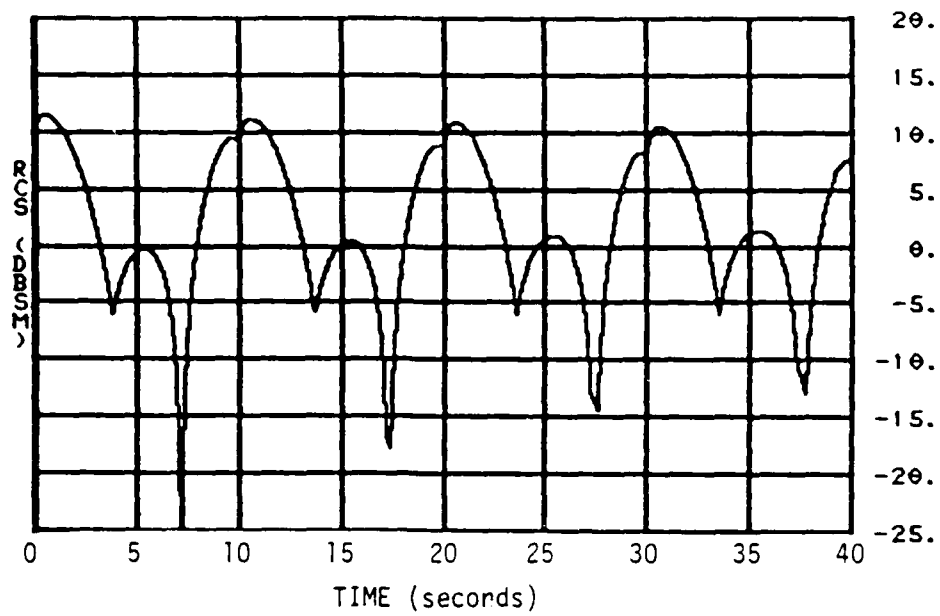


FIGURE 8. EFFECT OF PRECESSION ONLY ON THE EXAMPLE OBJECT

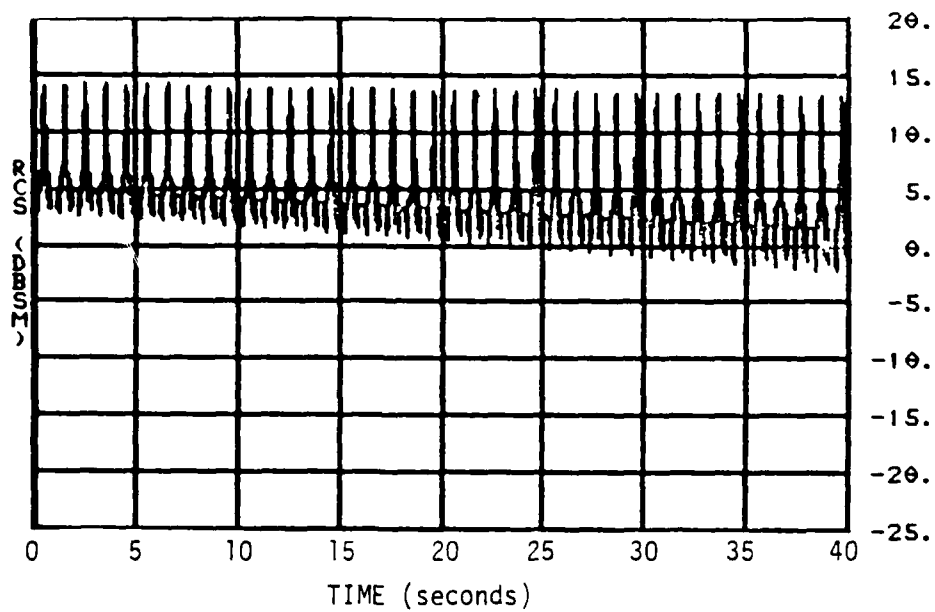


FIGURE 9. EFFECT OF SPIN ONLY ON THE EXAMPLE OBJECT

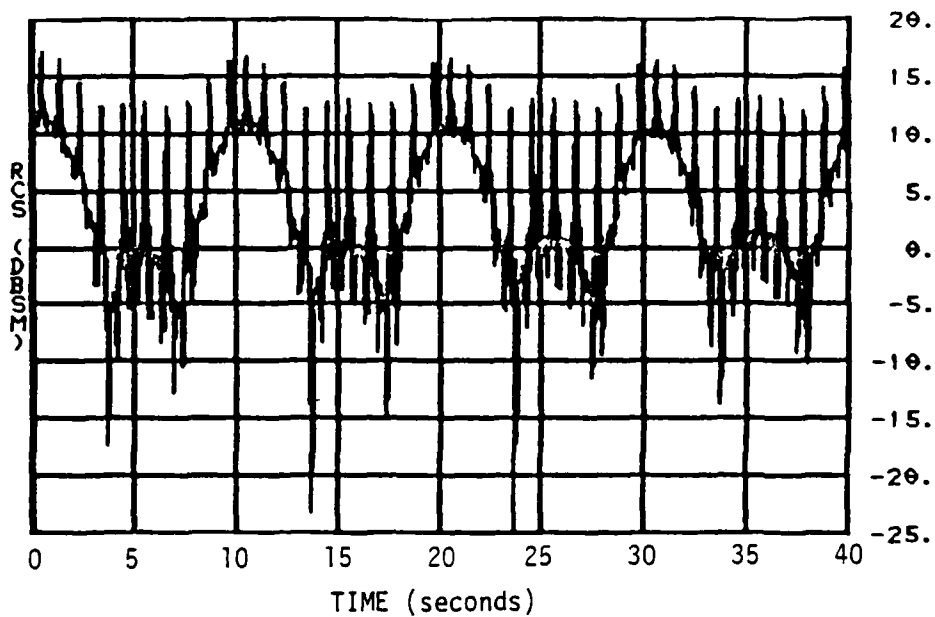


FIGURE 10. EFFECT OF BOTH SPIN AND PRECESSION ON THE EXAMPLE OBJECT

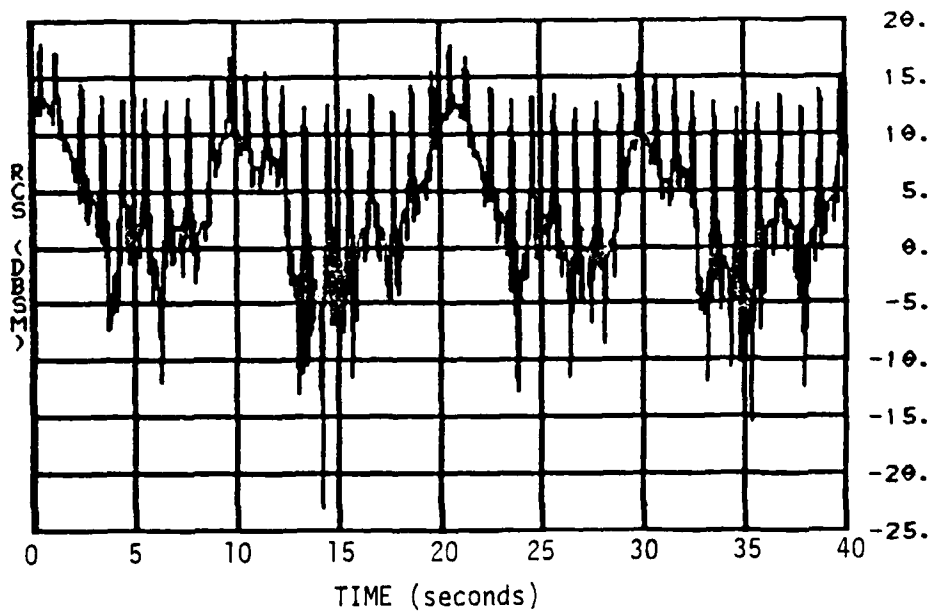


FIGURE 11. EFFECT OF SPIN, PRECESSION, AND NUTATION ON THE EXAMPLE OBJECT

TABLE 4. MSPB PARAMETERS USED IN THE EXAMPLE IMPLEMENTATION

SYMBOL	VALUE
A_1	2.0
A_2	0.006
A_3	0.00005
B_1	15.0
B_2	-0.7
B_3	0.003
\hat{P}_A	Vertical
PMA	0.07 (4 degrees)
AMA	$\pi/2$
α_0	0.05 (3 degrees)
β_0, γ_0	0
T_P	10 sec
T_S	2 sec
A_N	0.07 (4 degrees)
T_N	2 sec

path which has been modeled as the 2nd order polynomial in time. The combined effects of both spin and precession is shown in Figure 10, and a small nutation has been added in the data shown in Figure 11.

Thus this model is completely specified by the trajectory dependent and independent parameters of Tables 2 and 3, the main body RCS static pattern and an algorithm for the scatterer RCS. If the scatterer is allowed to move relative to the main body, a model of this relative motion is also required. The method for determining the composite RCS must also be specified for any given model.

APPENDIX A. DERIVATION OF THE TRANSFORMATION MATRICES (A AND D)

If two coordinate systems with a common origin are defined in space such that their respective axes do not coincide, the problem often arises of calculating the components of a vector in one system from the vector components as described in the second system. Such a conversion of vector components is called a transformation and is best described by:

$$V_i' = \sum_{j=1}^3 a_{ij} V_j \quad i = 1, 2, 3. \quad (A1)$$

The quantities (V_1, V_2, V_3) are defined as the components of the vector \vec{V} in the unprimed coordinate system. The second vector \vec{V}' is defined in terms of the transformation properties of its components under a rotation of the coordinate system. The a_{ij} are identified as the direction cosines of the angle as measured from the i -axis in the primed system to the j -axis in the unprimed system. A rectangular coordinate system can always be brought into coincidence with a second rectangular coordinate system with the same origin by rotating (transforming) about each orthogonal axis in turn and then combining the results. This information will now be used to derive the transformation matrices (A and D) used in Sections 3 through 5.

The transformation from the principle axis system to the motion axis system involves first a rotation of AMA degrees about the \hat{P} -axis (see Figure 5). The direction cosines for that rotation are:

$$\begin{aligned} b_{11} &= \cos (90 - AMA) = \sin (AMA) \\ b_{12} &= \cos (180 - AMA) = -\cos (AMA) \\ b_{13} &= \cos (90) = 0 \\ b_{21} &= \cos (AMA) \\ b_{22} &= \cos (90 - AMA) = \sin (AMA) \\ b_{23} &= \cos (90) = 0 \end{aligned} \quad (A2)$$

$$b_{31} = \cos (90) = 0$$

$$b_{32} = \cos (90) = 0$$

$$b_{33} = \cos (0) = 1.$$

A second rotation of PMA degrees about a-axis will bring the principle axis system in line with the motion axis system.

$$c_{11} = \cos (0) = 1$$

$$c_{12} = \cos (90) = 0$$

$$c_{13} = \cos (90) = 0$$

$$c_{21} = \cos (90) = 0$$

$$c_{22} = \cos (PMA) \tag{A3}$$

$$c_{23} = \cos (90 + PMA) = -\sin (PMA)$$

$$c_{31} = \cos (90) = 0$$

$$c_{32} = \cos (90 - PMA) = \sin (PMA)$$

$$c_{33} = \cos (PMA).$$

The total transformation is given by multiplying Equations (A2) by (A3).
Namely:

$$a_{ij} = \sum_{k=1}^3 c_{ik} b_{kj} \quad i = 1, 2, 3 \quad j = 1, 2, 3. \tag{A4}$$

The a_{ij} are the elements of transformation matrix \underline{A} which is then:

$$\underline{A} = \begin{pmatrix} \sin (AMA) & -\cos (AMA) & 0 \\ \cos (PMA) \cos (AMA) & \cos (PMA) \sin (AMA) & -\sin (PMA) \\ \sin (PMA) \cos (AMA) & \sin (PMA) \sin (AMA) & \cos (PMA) \end{pmatrix} \tag{A5}$$

Any vector \vec{V} can then be transformed from the principle axis coordinate system (unprimed) to the motion axis coordinate system (primed) using:

$$\vec{V}' = \underline{A} \cdot \vec{V} \tag{A6}$$

which is the equivalent of Equation (A1).

The transformation shown in Figure 3 is a standard Euler transformation*. The D -transformation is a rotation first about the $\hat{M}A$ -axis, second about the line of nodes, and finally about the new \hat{z} -axis. The elements of the D -matrix which will carry out the transformation from the motion axis system to the body coordinate system are listed in Equation (A7).

$$\begin{aligned}
 d_{11} &= \cos \gamma \cdot \cos \beta - \cos \alpha \cdot \sin \beta \cdot \sin \gamma \\
 d_{12} &= \cos \gamma \cdot \sin \beta + \cos \alpha \cdot \cos \beta \cdot \sin \gamma \\
 d_{13} &= \sin \gamma \cdot \sin \alpha \\
 d_{21} &= -\sin \gamma \cdot \cos \beta - \cos \alpha \cdot \sin \beta \cdot \cos \gamma \\
 d_{22} &= \cos \alpha \cdot \cos \beta \cdot \cos \gamma - \sin \gamma \cdot \sin \beta \\
 d_{23} &= \cos \gamma \cdot \sin \alpha \\
 d_{31} &= \sin \alpha \cdot \sin \beta \\
 d_{32} &= -\sin \alpha \cdot \cos \beta \\
 d_{33} &= \cos \alpha.
 \end{aligned} \tag{A7}$$

In the body coordinate system (double-primed) the \vec{V}'' is then:

$$\vec{V}_i'' = \sum_{k=1}^3 d_{ik} \vec{V}_k' \tag{A8}$$

or

$$\vec{V}'' = D \cdot \vec{V}'. \tag{A9}$$

The value of \vec{V}' [Equation (A6)] can be substituted into Equation (A9) to yield a direct transformation from the principle axis coordinate system to the body coordinate system.

$$\vec{V}'' = D \cdot A \cdot \vec{V}. \tag{A10}$$

*Goldstein, H., "Classical Mechanics", Addison-Wesley, 1965, pp. 107-109.

The vector \vec{V}'' has components which are properly defined in the (x, y, z) coordinate system shown in Figure 2. Namely:

$$\vec{V}'' = v_x \hat{x} + v_y \hat{y} + v_z \hat{z}. \quad (\text{A11})$$

Therefore the polar angle (θ_L) and the azimuth angle (ϕ_L) are then given by:

$$\theta_L = \cos^{-1} (v_z) \quad (\text{A12})$$

and

$$\phi_L = \tan^{-1} \left(\frac{v_y}{v_x} \right). \quad (\text{A13})$$

APPENDIX C

CORRELATED STATISTICAL (CORS) TIME VARYING RCS ALGORITHM

By
W. J. Gruner
L. K. Montgomery, Jr.

1. INTRODUCTION

TBE is required to develop exoatmospheric time varying L-band and UHF RCS models for objects of several weapons systems under Contract DASG60-79-C-0094. A statistical generation method is one procedure for simulating RCS histories that do not have significant time structure. TBE has developed a correlated statistical time varying RCS model for this purpose.

Section 2 presents a description of the correlated statistical time varying RCS model. This model has been used with Gaussian probability density functions and the parameters for this form of the model are given. Representative time histories are presented for several sets of input parameters.

2. CORRELATED STATISTICAL RCS GENERATION MODEL

The correlated statistical RCS generation model provides an RCS value given the last RCS value and the intervening time interval (Δt). It is represented mathematically by

$$RCS_{new} = p * RCS_{old} + (1-p) R$$

where $p = \exp(-COR * \Delta t)$ = correlation coefficient
and R = new random draw.

The exponential correlation function was based on the typical exponential decay observed in autocorrelation functions of RCS time histories. The underlying probability density is based on the observed data characteristics. Without additional constraints, this procedure can give unrealistic RCS values since mathematically the limits of a probability density may extend beyond physical reality. Thus the model provides a limit to the amount the RCS can change in a time interval and both upper and lower RCS limits.

A flow diagram of this model is shown in Figure 1. The random number R is drawn from the specified probability density. The bound is the maximum change in RCS allowed in the time interval Δt . RCS_{MAX} and RCS_{MIN} are specified to keep the RCS values within the realm of physical reality. When these limits are exceeded, the new RCS value is changed to stay within the specified limits.

The initial use of this model has been with the probability density defined as a Gaussian distribution in dBsm space. For the correlated Gaussian time varying RCS model, the six required parameters are given in Table 1. It was found to be convenient to define BOUND, RCS_{MAX} and

SYMBOL	PARAMETER DEFINITION
μ	Mean of Gaussian Density
σ	Standard Deviation of Gaussian Density
COR	Correlation Coefficient
BOUND	Maximum RCS Change in Δt
RCS_{MAX}	Maximum Allowed RCS Value
RCS_{MIN}	Minimum Allowed RCS Value

TABLE 1. CORRELATED GAUSSIAN TIME VARYING RCS MODEL PARAMETERS

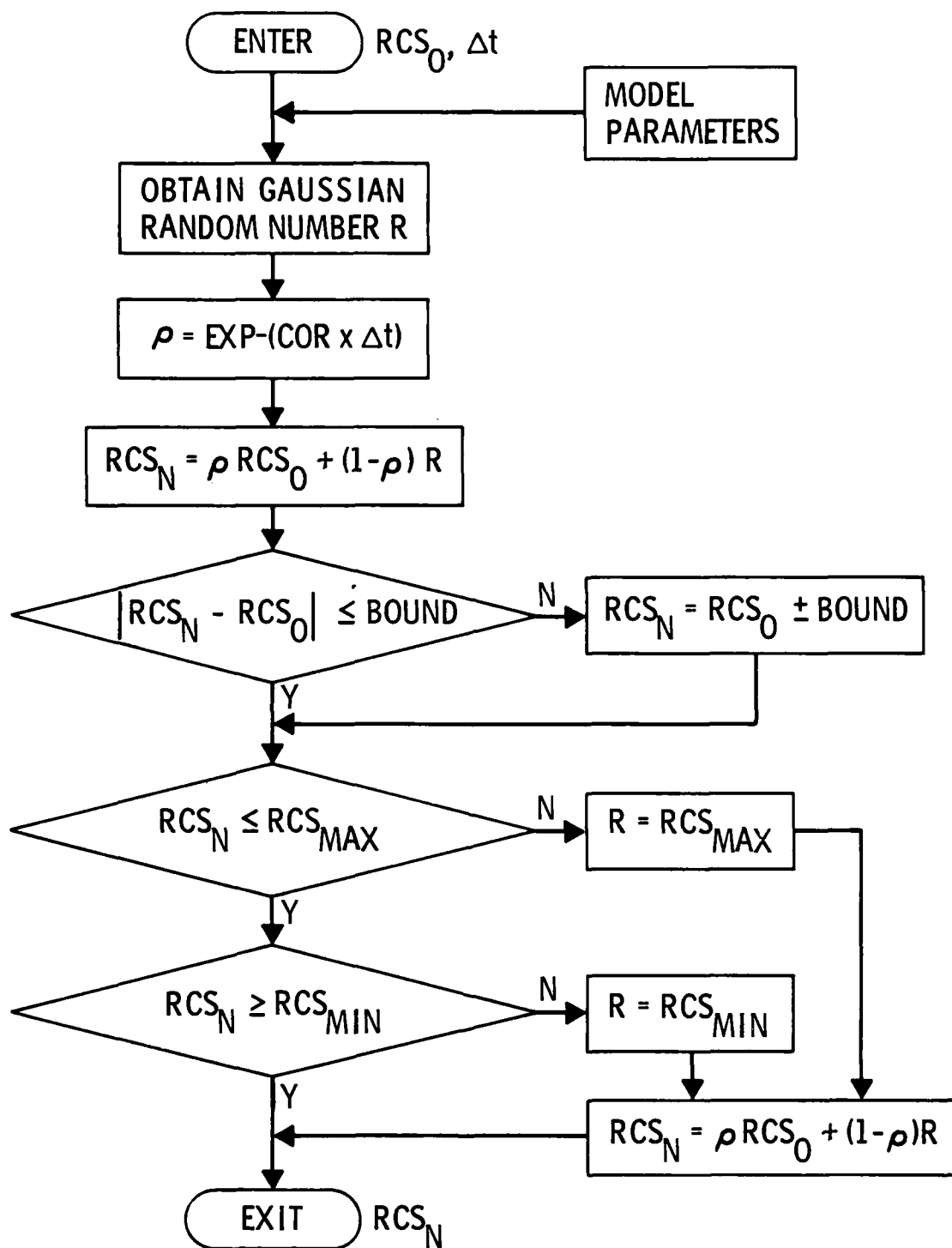


FIGURE 1. CORRELATED STATISTICAL TIME VARYING RCS MODEL

RCS_{MIN} in terms of μ and σ as

$$BOUND = NUM * \sigma * \exp(\Delta t)$$

$$RCS_{MAX} = \mu + NSU * \sigma$$

$$RCS_{MIN} = \mu - NSL * \sigma.$$

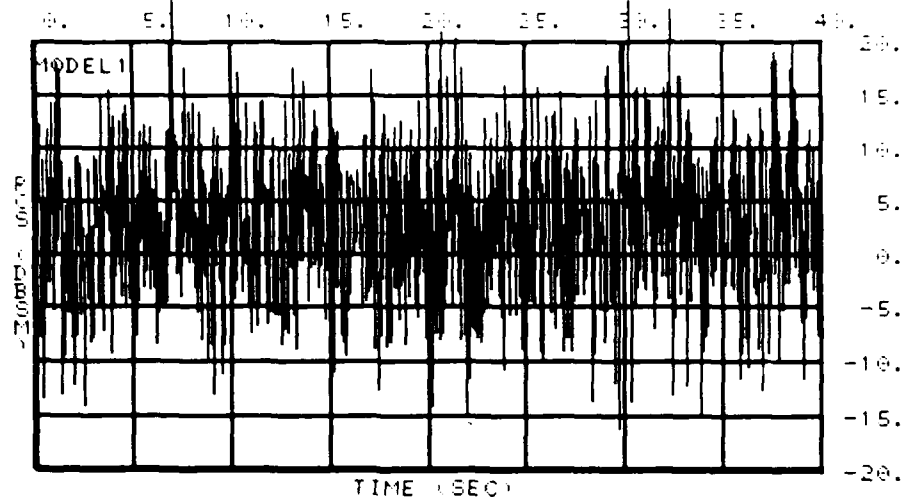
Thus for the correlated Gaussian model, the six parameters are μ , σ , COR, NUM, NSU, and NSL. To model a particular object, these parameters will in general be defined as probability distributions.

In developing this model it was found necessary to expand the Gaussian density for highly correlated draws (i.e. small values of COR and Δt). This expansion is accomplished by using $\sigma^1 = \sigma / \text{FACTOR}$ instead of σ as the standard deviation of the Gaussian distribution where

$$\text{FACTOR} = \begin{cases} 1 & ; \text{COR} * \Delta t \geq 2.86 \\ 0.6056 * \log_{10}(\text{COR} * \Delta t) + 0.723 & ; \text{otherwise} \end{cases}$$

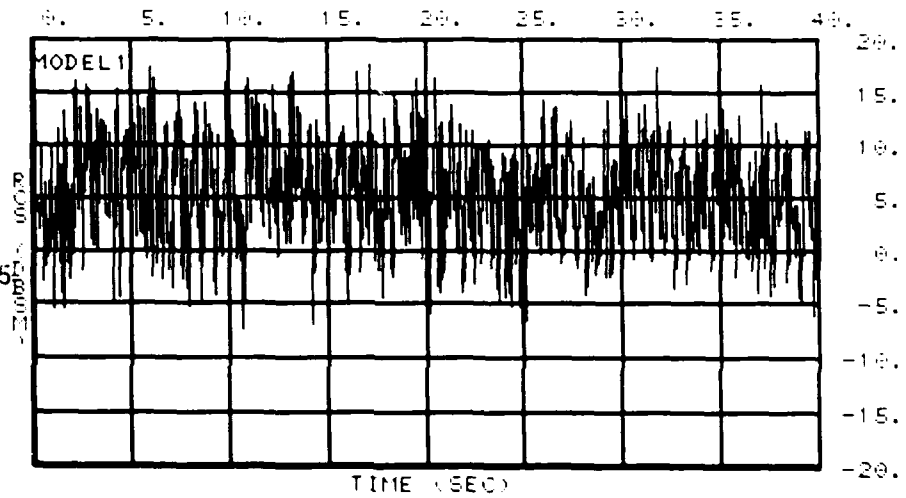
Examples of the model output for selected values of the parameters are shown in Figure 2. These data were generated at 24 Hz. More structure is seen in Figure 2(c) which has the smallest correlation coefficient and standard deviation of the cases illustrated.

$\mu = 3$
 $\sigma = 7$
COR = 100
NUM = 4
NSU = NSL = 3



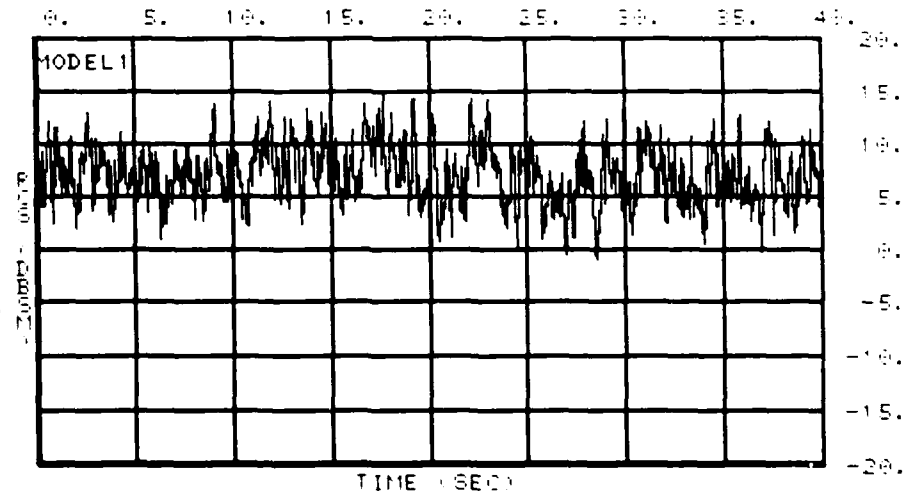
(a)

$\mu = 5$
 $\sigma = 5$
COR = 25
NUM = 3.75
NSU = NSL = 2.5



(b)

$\mu = 7$
 $\sigma = 3$
COR = 10
NUM = 3.5
NSU = NSL = 2.7



(c)

FIGURE 2. CORRELATED GAUSSIAN RCS MODEL

APPENDIX D

SINUSOIDS AND RANDOM PROCESS (SARP)
TIME VARYING RCS ALGORITHM

By
W. J. Gruner

1. INTRODUCTION

TBE is required to develop exoatmospheric time varying L-band and UHF RCS models for objects of several missile systems under Contract DASG60-79-C-0094. TBE has developed SARP for the simulation of RCS time histories from objects with significant time structure and without definable motion characteristics. SARP provides simulated RCS values by the sum of harmonically related sinusoids and an uncorrelated random process in dBsm space.

Section 2 presents a description of SARP. Model parameters, generation variables, and constraints are discussed. Representative time histories are presented for several sets of input parameters.

2. RCS GENERATION MODEL SARP

SARP provides an RCS value at a specified time given sinusoidal amplitudes, frequencies, initial phases, and relative random process components. A diagram of SARP is shown in Figure 1. The returned RCS value in dBsm is expressed mathematically as:

$$RCS = \mu + R_S + R_N$$

where

μ is the desired mean value

R_S is the sinusoidal component

from NSIN harmonically related sinusoids,

R_N is a Gaussian-distributed random component.*

These variables are functionally related to the required SARP model parameters in Table 1. Some of these parameters - μ , VAR, RELN, and F_0 - would generally be specified in terms of probability density functions to provide the variability between various observations of the same object. The number of sinusoids (NSIN), relative amplitudes (AMPN) and initial phase (PHAS) are determined from power spectral density analyses of measured RCS history data.

The SARP random variable R_N is a zero mean Gaussian random variable* with standard deviation σ_N . Since mathematically, the limits of this distribution can extend beyond physical reality, the value of R_N is constrained by $|R_N| \leq 3\sigma_N$. The standard deviation is related to the parameters RELN and VAR by

$$\sigma_N = 10 \text{ (RELN/10)} * \text{VAR}^{1/2}$$

where R_N and σ_N have the units of dBsm. The relative random process component (RELN) is constrained by $\text{RELN} \leq 0$. If $\text{RELN} = 0$ there is no

* If appropriate, other probability density functions could be used for R_N . However, all applications to date by TBE have used Gaussian probability density functions so the model is described in this manner.

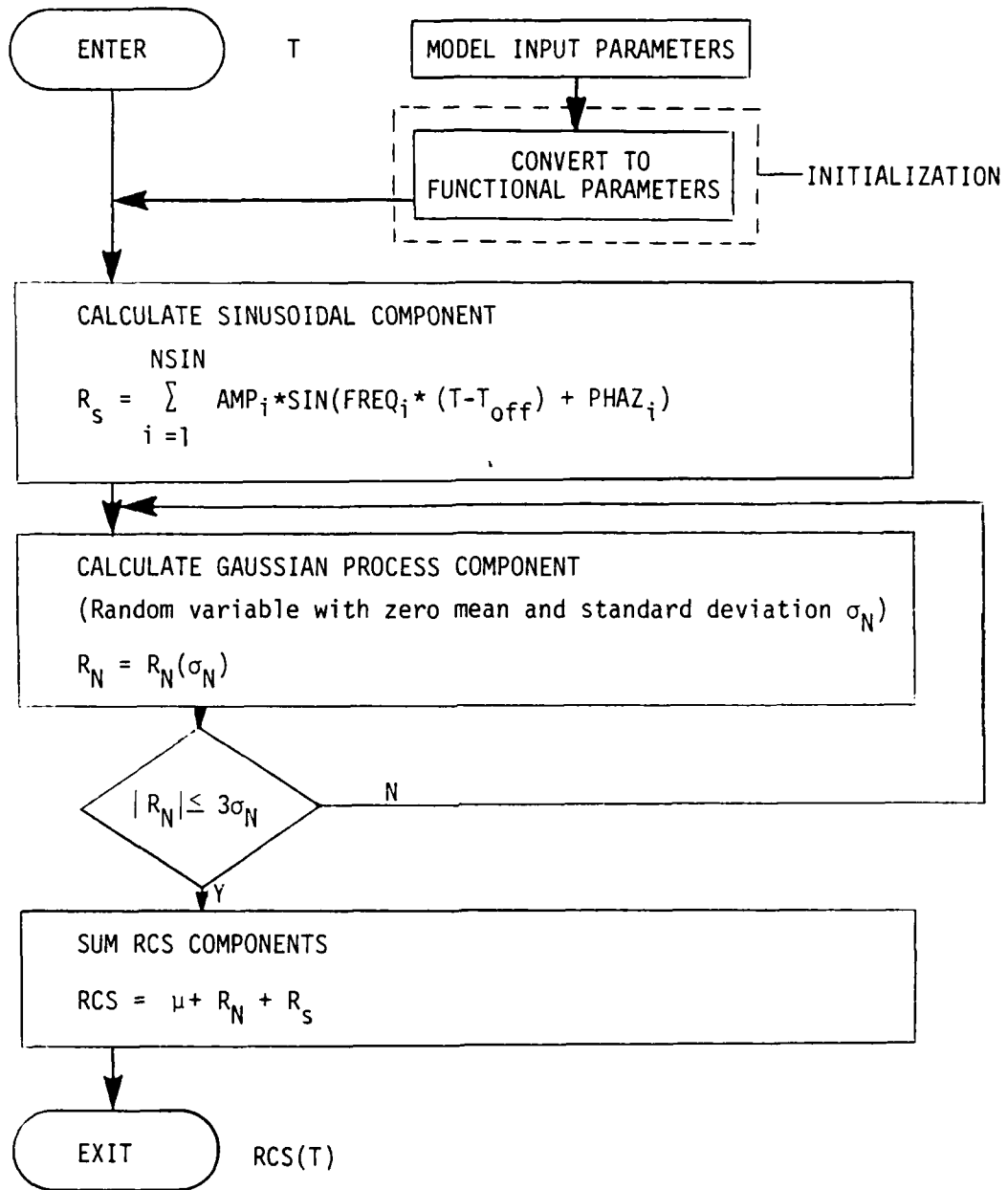


FIGURE 1. TIME VARYING RCS GENERATION MODEL SARP

TABLE 1. SARP TIME VARYING RCS MODEL PARAMETERS

SYMBOL	PARAMETER
μ	Process mean (dBsm)
VAR	Process variance (dBsm ²)
RELN	Relative random process component (dB relative to composite)
F_0	Sinusoidal component fundamental frequency (Hz)
NSIN	Number of harmonically related sinusoids (unitless)
AMPN	Array of sinusoidal amplitudes normalized relative to sinusoidal composite (unitless)
PHAS	Array of sinusoidal initial phase (deg)

TABLE 2. EXAMPLE SARP SINUSOIDAL INPUT, NSIN = 4

HARMONIC	AMPN	PHAS (deg)
1	1.20	70
2	.66	- 10
3	.32	- 90
4	.10	-140

sinusoidal component and the simulation consists of a constrained uncorrelated random process.

The SARP sinusoidal component R_s is determined by

$$R_s = \sum_{i=1}^{NSIN} AMP_i * \sin(FREQ_i * (T - T_{off}) + PHAZ_i)$$

Where $AMP_i = AMPN_i * (VAR * 1. - 10^{RELN/10})^{1/2}$

is the sinusoidal amplitude (dBsm)

$$FREQ_i = i * F_o * 2\pi$$

is the sinusoidal frequency (rad/sec)

T_{off} is a uniform initial bias time drawn from the interval $(0, 1/F_o)$

$$PHAZ = \frac{2\pi}{360} (PHAS)$$

is the sinusoidal initial phase (rad) at time $T = 0$.

Physical constraints are modeled by limiting the amplitude densities associated with μ , VAR, RELN and F_o .

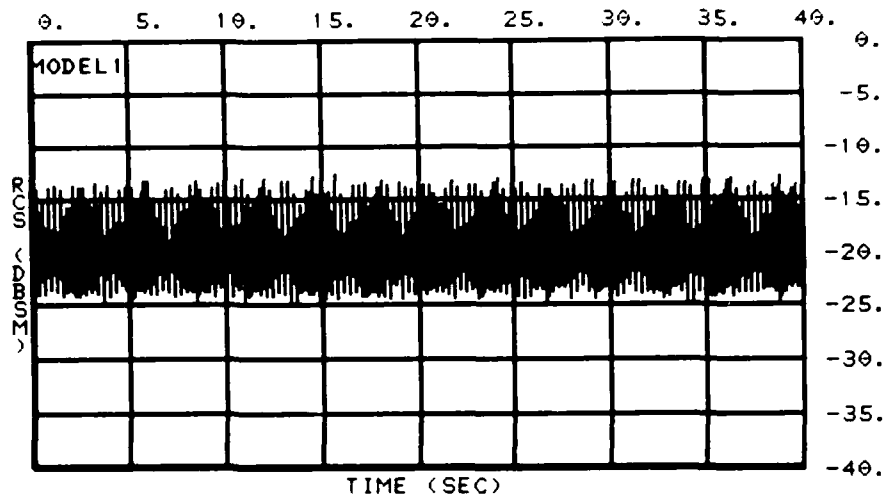
Examples of SARP output for selected input parameters are shown in Figure 2. These figures were generated with $NSIN = 4$ and values for relative amplitudes and initial phase angle are given in Table 2.

These data were generated at the indicated data rates. More structure is seen as RELN is decreased. Figures 2(a) - (c) are 40-second realizations sampled at a constant data rate of 24 Hz. Figure 2(a) is predominantly sinusoidal with $RELN = -20$ dB and $F_o = 3.31$ Hz. Figures 2(b) and 2(c) were generated with $F_o = 1.83$ Hz and $RELN = -10$ and -2 . With $RELN = -2$ the structure of the simulated pattern is predominantly random. Figures 2(d) - (f) are 200-second realizations of the same processes as used in Figures 2(a) - (c) but with much lower data rates of 1 Hz in Figure 2(d) and 0.5 Hz in Figures 2(e) and 2(f). In these figures the sinusoidal pattern is also shifted by $T_{off} = 0.5$ sec at simulation time zero.

Figure 3 shows SARP realizations at time intervals corresponding to non-uniform data rates obtained on an object for which SARP has been used. The parameters incorporated in SARP for Figures 3(a) and 3(b) are

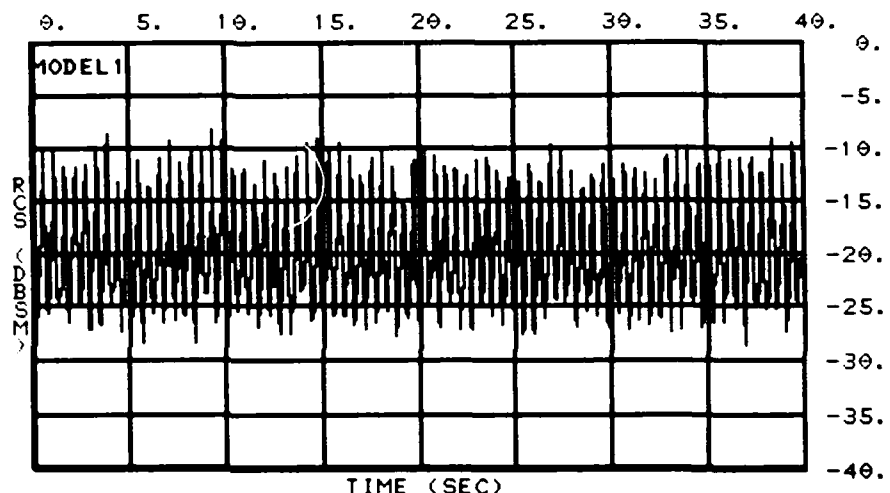
identical. With the relative random noise (RELN) at -4 dB, the sinusoidal and the random components contribute approximately 60% and 40% in terms of RCS variance. The average data rate in Figure 3(a) is approximately 15 Hz over an interval of nearly 40 seconds and the average data rate in Figure 3(b) is 0.67 Hz over an interval of approximately 170 seconds. In the figures, the irregular sampling causes the simulated histories to appear predominantly random. In Figure 3(b), if a sinusoidal process were postulated, an observer might deduct an apparent frequency of 0.1 Hz as opposed to the true SARP fundamental periodicity associated with 3.31 Hz.

$\mu = -20$
 $\text{VAR} = 10$
 $\text{RELN} = -20$
 $F_0 = 3.31$
 $T_{\text{off}} = 0.0$



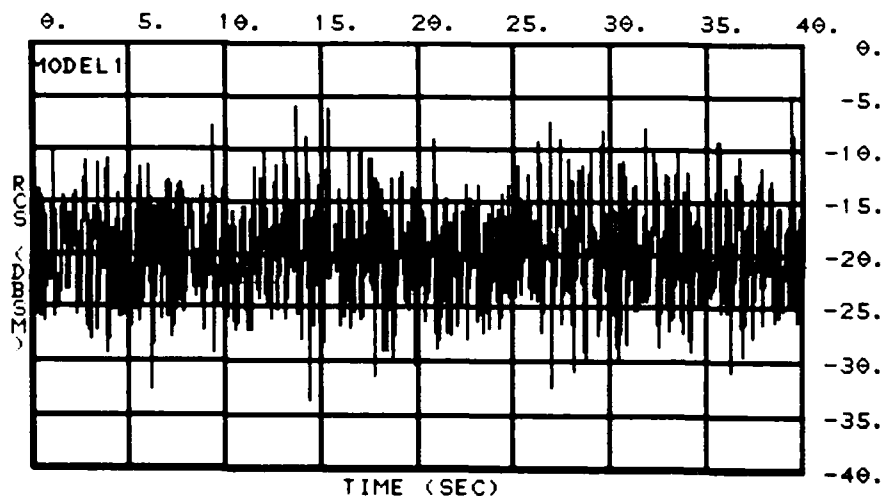
(a) 24 Hz Data Rate

$\mu = -20$
 $\text{VAR} = 20$
 $\text{RELN} = -10$
 $F_0 = 1.83$
 $T_{\text{off}} = 0.0$



(b) 24 Hz Data Rate

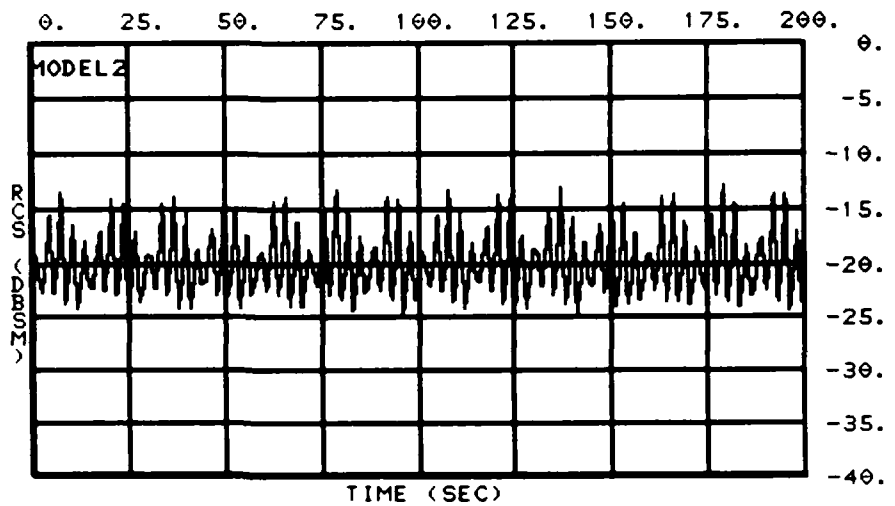
$\mu = -20$
 $\text{VAR} = 20$
 $\text{RELN} = -2$
 $F_0 = 1.83$
 $T_{\text{off}} = 0.0$



(c) 24 Hz Data Rate

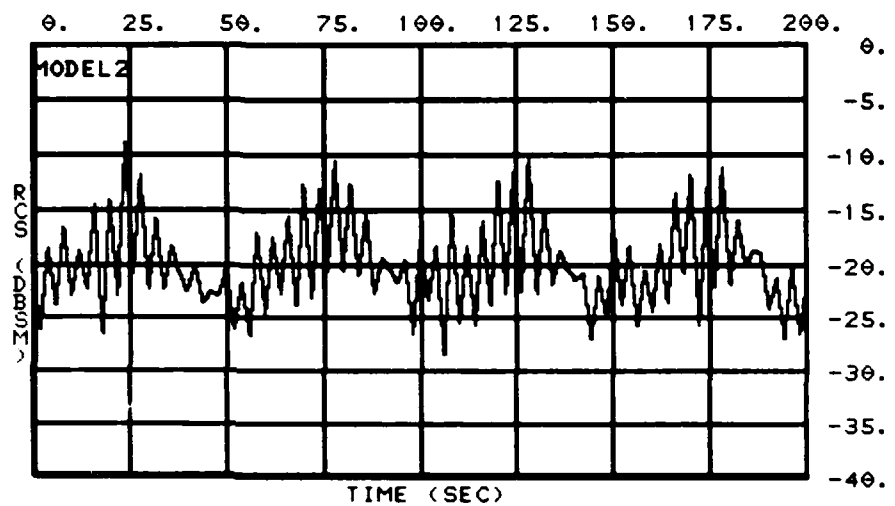
FIGURE 2. EXAMPLE SARP RCS REALIZATIONS, SAMPLING AT CONSTANT DATA RATES

$\mu = -20$
 $VAR = 10$
 $RELN = -20$
 $F_0 = 3.31$
 $T_{off} = 0.5$



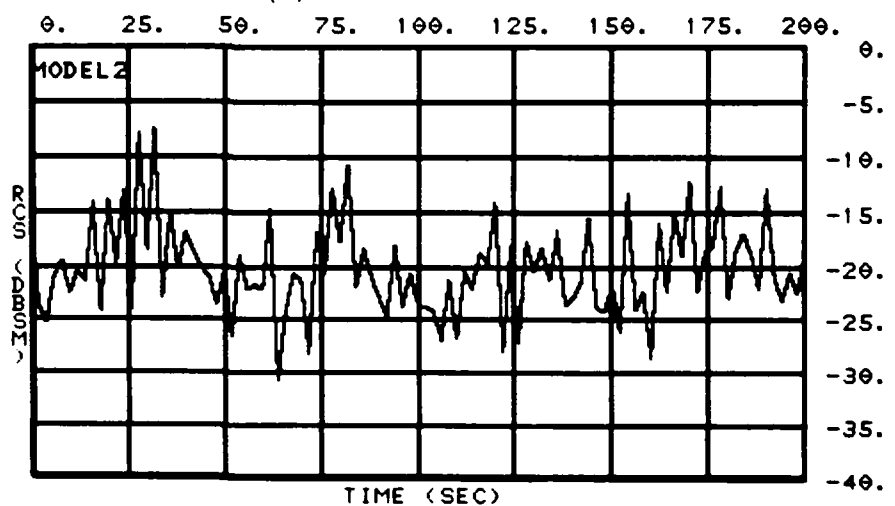
(d) 1 Hz Data Rate

$\mu = -20$
 $VAR = 20$
 $RELN = -10$
 $F_0 = 1.83$
 $T_{off} = 0.5$



(e) 0.5 Hz Data Rate

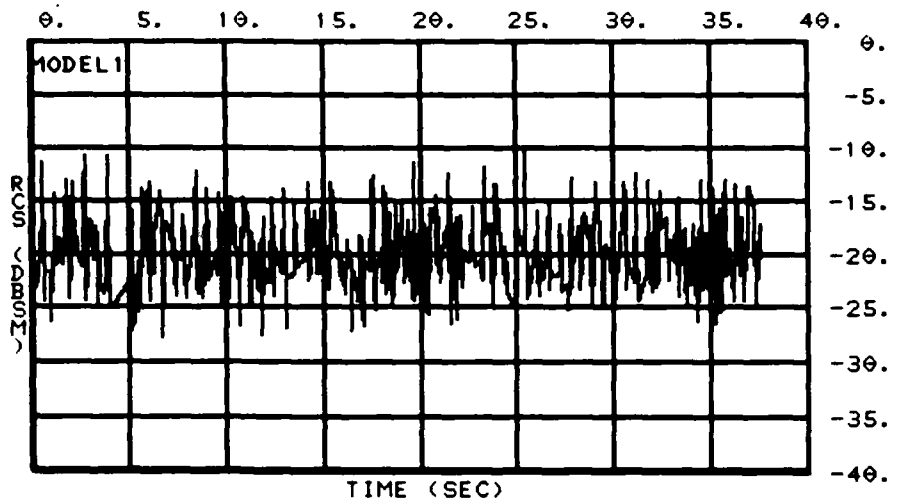
$\mu = -20$
 $VAR = 20$
 $RELN = -2$
 $F_0 = 1.83$
 $T_{off} = 0.5$



(f) 0.5 Hz Data Rate

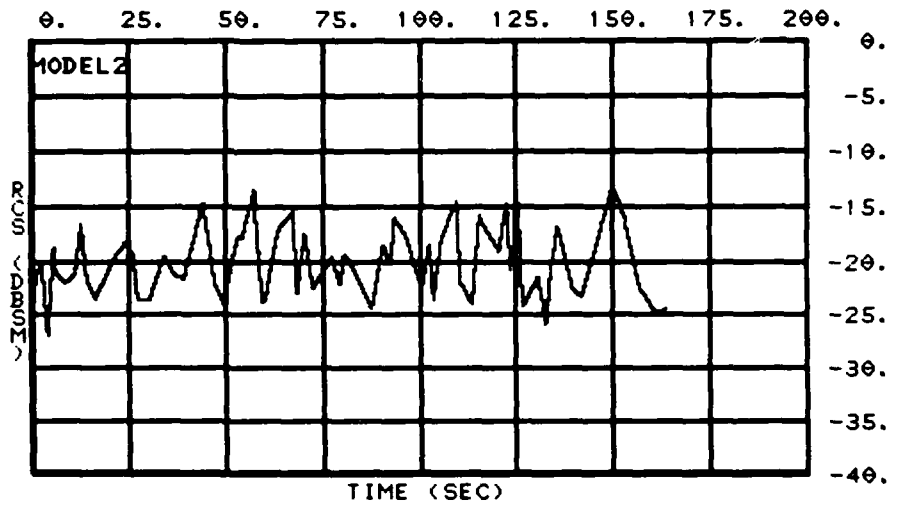
FIGURE 2. EXAMPLE SARP RCS REALIZATIONS, SAMPLING AT CONSTANT DATA RATES (CONCLUDED)

$\mu = -20$
 $VAR = 10$
 $RELN = -4$
 $F_0 = 3.31$
 $T_{off} = 0.0$



(a) ≈ 15 Hz Data Rate

$\mu = -20$
 $VAR = 10$
 $RELN = -4$
 $F_0 = 3.31$
 $T_{off} = 0.0$



(b) ≈ 0.67 Hz Data Rate

FIGURE 3. EXAMPLE SARP RCS REALIZATIONS, SAMPLING AT NON-UNIFORM DATA RATES

APPENDIX E

MODIFIED SINUSOIDS AND RANDOM PROCESS (MSARP)
TIME VARYING RCS ALGORITHM

By
W. J. Gruner

1. INTRODUCTION

TBE is required to develop exoatmospheric time varying L-band and UHF RCS models for objects of several missile systems under Contract DASG60-79-C-0094. TBE has developed MSARP for the simulation of RCS time histories from complex objects with significant time structure and without definable motion characteristics. MSARP provides simulated RCS values by the sum of related sinusoids and an uncorrelated random process in dBsm space as provided by SARP (Appendix D). MSARP expands the concept of SARP by randomly selecting higher frequency components.

Section 2 presents a description of MSARP. Model parameters, generation variables, and constraints are discussed. Representative time histories are presented for several sets of input parameters.

2. RCS GENERATION MODEL MSARP

MSARP provides an RCS value at a specified time based on sinusoidal amplitudes, frequencies, initial phases, and relative random process components. A diagram of MSARP is shown in Figure 1. The returned RCS value in dBsm is expressed mathematically as:

$$\text{RCS} = \mu + R_S + R_N$$

where

μ is the desired mean value,

R_S is the sinusoidal component

from NSIN sinusoids,

R_N is a Gaussian-distributed random component.

These variables are functionally related to the required MSARP model parameters in Table 1. Some of these parameters (μ , VAR, RELN, and F_0) would generally be specified in terms of probability density functions to provide the variability between various observations of the same object.

The MSARP random variable R_N is a zero mean Gaussian random variable* with standard deviation σ_N . Since mathematically, the limits of this distribution can extend beyond physical reality, the value of R_N is constrained by $|R_N| \leq 3\sigma_N$. The standard deviation is related to the parameters RELN, VAR, and R_S by

$$\sigma_N = \text{MAX} \left\{ 0.01, 1.8 \left(10^{(\text{RELN}/10)} * \text{VAR}^{1/2} \right) (0.85 - 0.04 * R_S) \right\}$$

where R_N and σ_N have the units of dBsm.* The relative random process component (RELN) is constrained by $\text{RELN} \leq 0$. If $\text{RELN} = 0$ there is no sinusoidal component and the simulation consists of a constrained uncorrelated random process.

For MSARP, the number of sinusoids is randomly chosen from a uniform density with a specified range. This range is derived from power spectral density analyses of the associated data. The sinusoidal frequencies are chosen to be nonharmonic by a small random component. For example,

*If appropriate, other probability density functions could be used for R_N . However, all applications to date by TBE have used Gaussian probability density functions so the model is described in this manner.

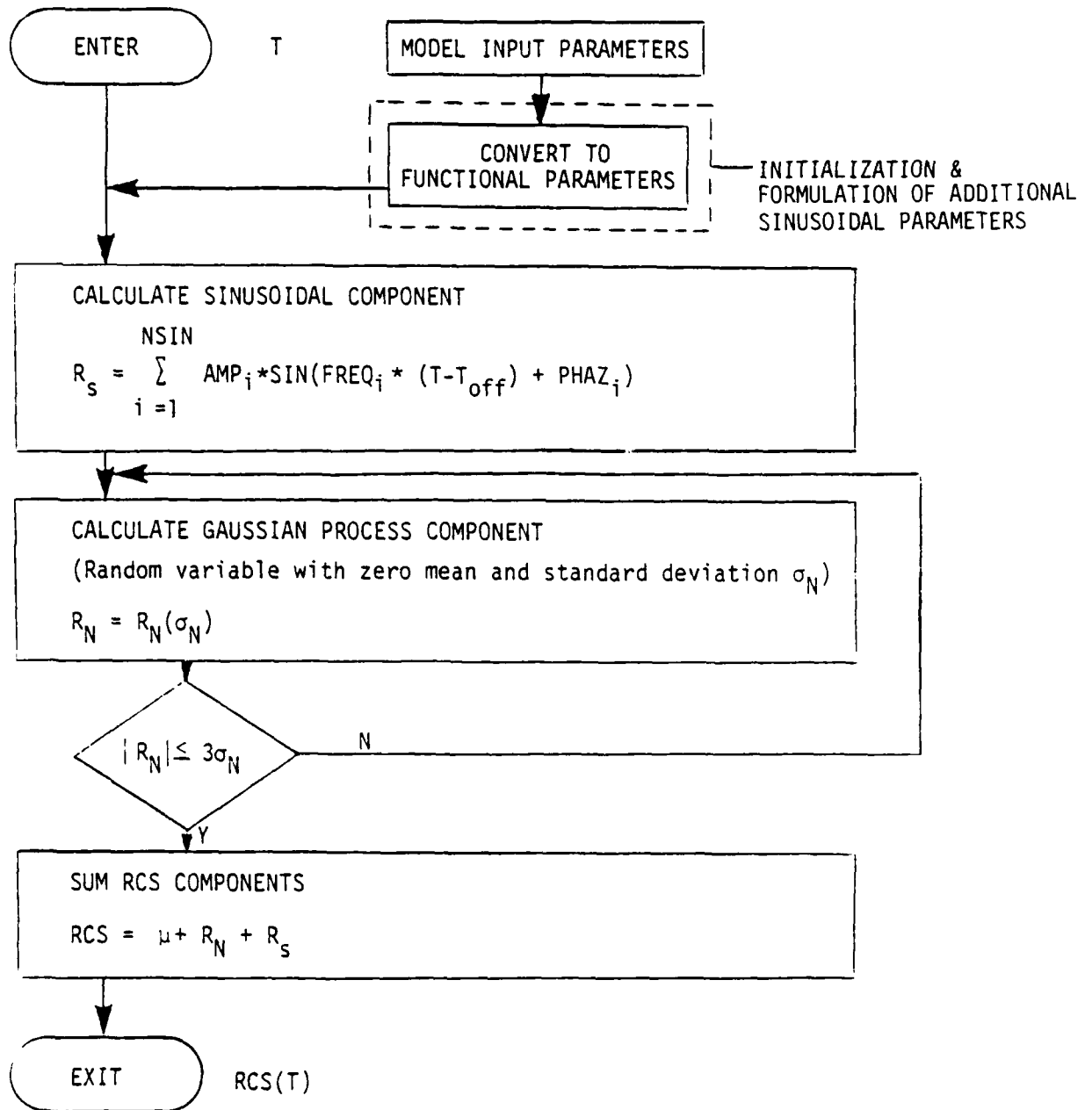


FIGURE 1. TIME VARYING RCS GENERATION MODEL MSARP

TABLE 1. MSARP TIME VARYING RCS MODEL PARAMETERS

SYMBOL	PARAMETER
μ	Process mean (dBsm)
VAR	Process variance (dBsm ²)
RELN	Relative random process component (dB relative to composite)
F_0	Sinusoidal component fundamental frequency (Hz)
NSIN	Number of sinusoids (unitless)
AMPN	Array of relative sinusoidal amplitudes for initial subset of sinusoids (unitless)
σ_F	Standard deviation of frequency non-harmonic component
σ_A	Standard deviation of sinusoidal amplitude random component

Logical expression for amplitudes of sinusoids of higher order than initial subset, relative to final specified amplitude. This expression is prior to application of random component. For example

$$\text{AMPN}(I) = \text{AMPN}(J) (1.0 - 1.1 \log_{10} (I/J)), J < I \leq \text{NSIN}$$

where J sinusoids were specified in the initial subset

$$F_i = \Gamma_o * (1 + F_N) * i$$

where F_N is a zero-mean Gaussian distributed random variable with a specified standard deviation, σ_F , constrained to be within $\pm 3\sigma_F$.

Relative sinusoidal amplitudes for an initial subset of sinusoids are determined directly from the power spectral density analyses. The power spectral densities are also used to derive a logical relationship for establishing the amplitude of the sinusoids. This logical relationship is determined in the form of average relative amplitude vs frequency. The actual amplitude is then derived as the deterministic average amplitude plus a random component where amplitude is also determined from power spectral density analysis. For example, if 8 sinusoidal amplitudes have been determined the amplitudes of the remaining NSIN - 8 sinusoids may be determined by

$$AMPN_i = \text{MAX} \left\{ 0.01, \text{AMPA} * \text{AMPN}_8 \times (1.0 - 1.1 \log_{10}(i/8)) \right\}$$

where $\text{AMPA} = \text{MAX} \left\{ 1. + \text{AMPSI6} \right\}$

and AMPSI6 is a zero mean Gaussian random variable with standard deviation σ_A with amplitude constrained to $3\sigma_A$. After all relative amplitudes have been calculated, they are normalized to produce the desired variance. For MSARP, all initial phase angles (PHAZ_i) are chosen from a uniform density ranging from 0 to 2π radians.

The MSARP sinusoidal component R_s is determined identically to the SARP technique by

$$R_s = \sum_{i=1}^{\text{NSIN}} \text{AMP}_i * \text{SIN} (\text{FREQ}_i * (T - T_{\text{off}}) + \text{PHAZ}_i)$$

where $\text{AMP}_i = \text{AMPN}_i * (\text{VAR} * \{1. - 10^{\text{RELN}/10}\})^{1/2}$
is the sinusoidal amplitude (dBsm)

T_{off} = is a uniform initial time bias drawn from the interval $(0, 1/F_o)$

$$\text{FREQ}_i = F_i * 2\pi$$

is the sinusoidal frequency (rad/sec)

Physical constraints are modeled by limiting the amplitude densities associated with μ , VAR, RELN and F_o .

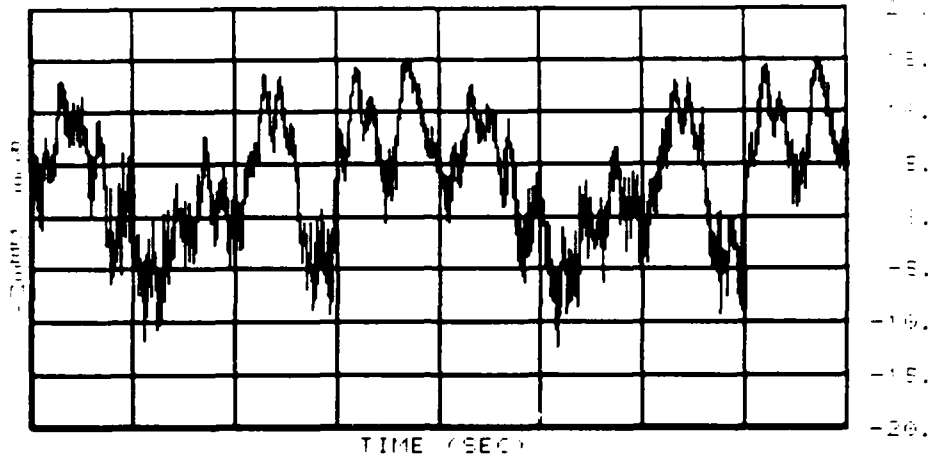
Example MSARP outputs for the parameters of Table 2 are shown in Figure 2. All realizations were derived at constant values of μ , VAR, and RELN. Figures 2 (a-c) were generated at a fundamental frequency of 0.025 Hz and Figures 2 (d-f) at a fundamental frequency of 0.010 Hz. All data are formulated for a period of 80 seconds at a constant 20 Hz data rate. These examples are repetitive except for the random component in the period associated with the fundamental frequency, and can be used to simulate complex scatters.

TABLE 2. EXAMPLE MSARP INPUT
(INITIAL SINUSOIDAL INPUT FOR 8 FREQUENCIES)

SINUSOIDAL	1	2	3	4	5	6	7	8
AMPN	.76	.53	.41	.45	.42	.54	.23	.50
AMPN(I) = AMPN (8) · (1.0 - 1.1 log ₁₀ (I/8)), I > 8								

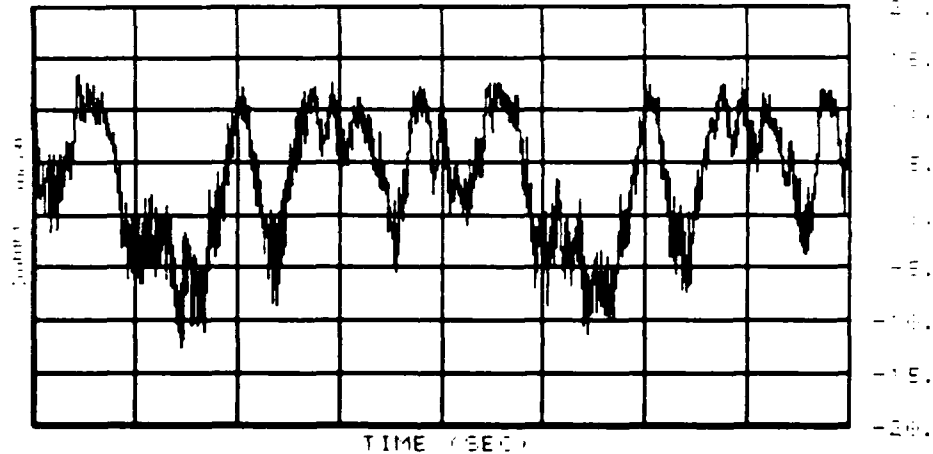
σ
 A = 0.2
 σ
 F = 0.0016

$\mu = 3.5$
 VAR = 32.5
 RELN = -14.0
 $F_0 = 0.025$
 NSIN = 32
 $T_{off} = 0.0$



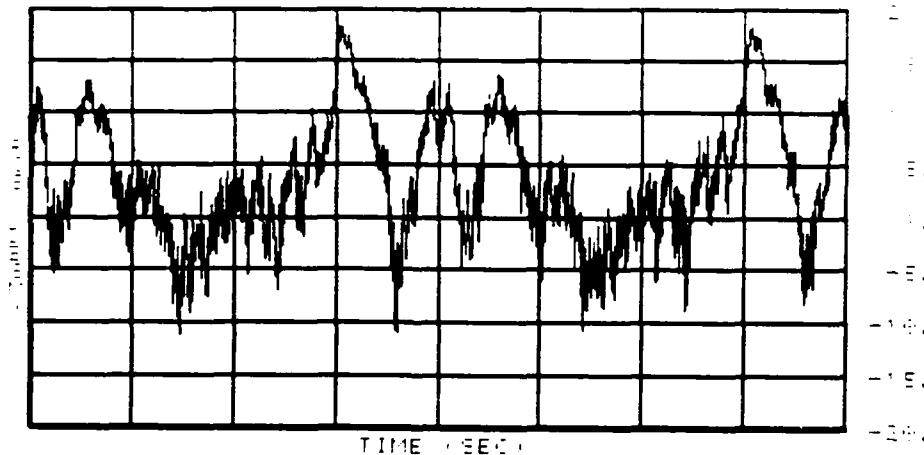
(a) 20 Hz Data Rate

$\mu = 3.5$
 VAR = 32.5
 RELN = -14.0
 $F_0 = 0.025$
 NSIN = 44
 $T_{off} = 0.0$



(b) 20 Hz Data Rate

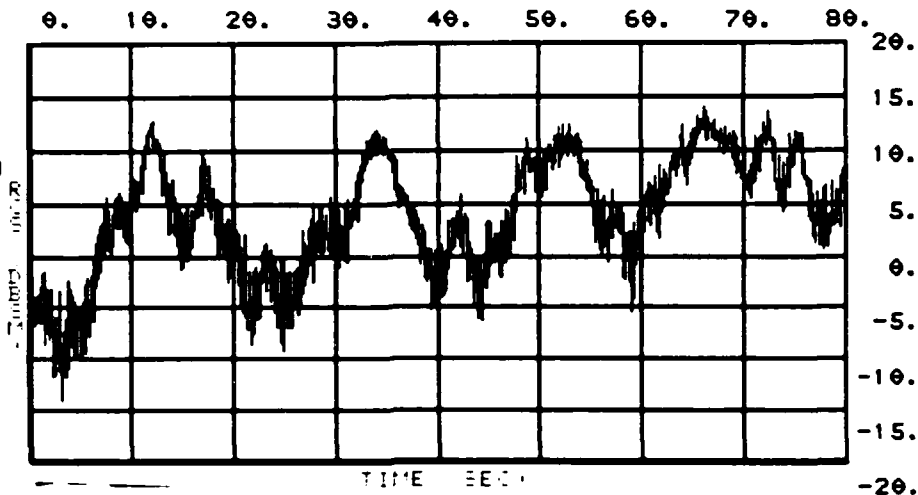
$\mu = 3.5$
 VAR = 32.5
 RELN = -14.0
 $F_0 = 0.025$
 NSIN = 50
 $T_{off} = 0.0$



(c) 20 Hz Data Rate

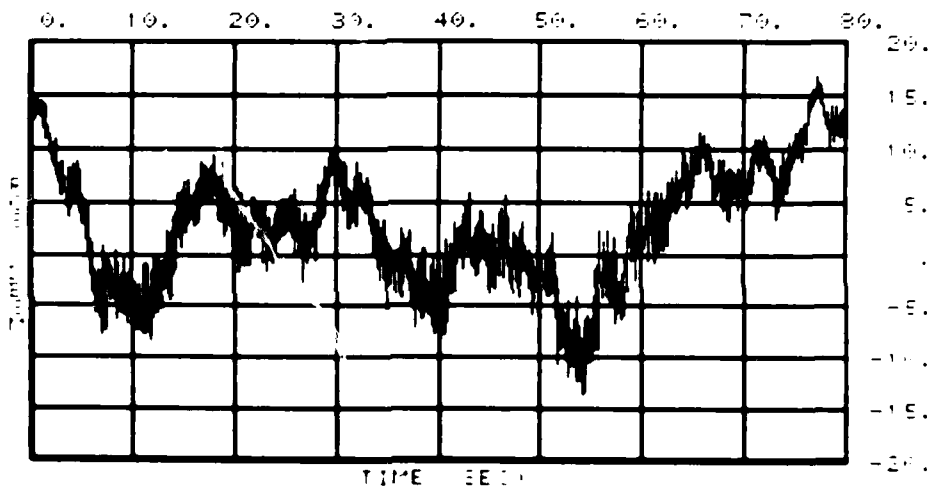
FIGURE 2. EXAMPLE MSARP REALIZATIONS, SAMPLING AT CONSTANT DATA RATES

$\mu = 3.5$
 $VAR = 32.5$
 $RELN = -14.0$
 $F_o = 0.010$
 $NSIN = 41$
 $T_{off} = 0.0$



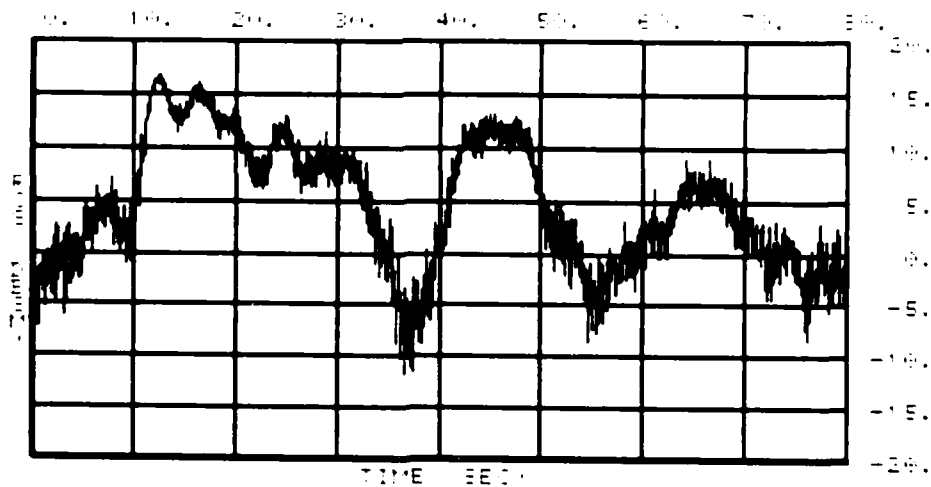
(d) 20 Hz Data Rate

$\mu = 3.5$
 $VAR = 32.5$
 $RELN = -14.0$
 $F_o = 0.010$
 $NSIN = 46$
 $T_{off} = 0.0$



(e) 20 Hz Data Rate

$\mu = 3.5$
 $VAR = 32.5$
 $RELN = -14.0$
 $F_o = 0.010$
 $NSIN = 31$
 $T_{off} = 0.0$



(f) 20 Hz Data Rate

FIGURE 2. CONCLUDED

UNCLASSIFIED

DISTRIBUTION LIST (U)

<u>Names and Addresses</u>	<u>Number of Copies</u>
Assistant Secretary of Air Force Research, Development and Logistics Deputy for Strategic and Space Systems Pentagon Washington, D.C. 20330 ATTN: Henry F. Cooper, SAFALR	1
Aerospace Defense Center Peterson AFB, Colorado 80914 ATTN: ADC/XPY, J. Darrah	1
Air Force Systems Command Andrews Air Force Base Washington, D.C. 20331 ATTN: INA, COL K. Negus XRK, MAJ Ellen	1 1
Air Force Weapons Laboratory Kirkland Air Force Base New Mexico 87117 ATTN: NTN, Mr. Gordon	1
Commander Ballistic Missile Defense Systems Command P.O. Box 1500 Huntsville, Alabama 35807 ATTN: BMDSC-HI BMDATC-D, Jim Karr	2 1
4602 CPUSS/ADBTS Peterson AFB, Colorado 80914 ATTN: CPT Capp	1
Command and Control Technical Center/DCA BE 685, The Pentagon Washington, D.C. 20301 ATTN: Mr. J. A. Hoff (C605H)	1
Defense Intelligence Agency Washington, D.C. 20301 ATTN: DT-2, Jim Miller	1

DL-1

UNCLASSIFIED

UNCLASSIFIED

DISTRIBUTION LIST - Continued (U)

<u>Names and Addresses</u>	<u>Number of Copies</u>
Director Defense Nuclear Agency Washington, D.C. 20305 ATTN: NAFD, MAJ Williamson	1
Defense Technical Information Center Cameron Station Alexandria, Virginia 22314	2
Headquarters, ESD Mail Stop 10 Hanscom AFB, Massachusetts 01731 ATTN: ESD/XRW, COL M. F. Burke	4
The Joint Chiefs of Staff/SAGA Pentagon Washington, D.C. 20301 ATTN: LTC Chrobak	1
The Joint Chiefs of Staff/J3 Pentagon Washington, D.C. 20301 ATTN: Strategic Operations Division, COL Smith	1
Foreign Technology Division Wright-Patterson AFB, Ohio 45433 ATTN: SDBG, A. Whitehill	3
National Security Agency/W15 Fort Meade, Maryland 20755	1
Naval Intelligence Support Center 4301 Suitland Road Washington, D.C. 20390 ATTN: NISC/4121, Jim Hyland	1
HQ SAC/ADS Offutt Air Force Base, Nebraska 68113	1
HQ SAC/DOCW Offutt Air Force Base, Nebraska 68113 ATTN: LTC Wakefield	1
HQ SAC/SX Offutt Air Force Base, Nebraska 68113	1

DL-2

UNCLASSIFIED

UNCLASSIFIED

DISTRIBUTION LIST - Continued (U)

<u>Names and Addresses</u>	<u>Number of Copies</u>
HQ SAC/XP Offutt Air Force Base, Nebraska 68113	1
HQ Space Division P.O. Box 92960 World Way Postal Center Los Angeles, California 90009 ATTN: INK, MAJ D. Tuntland	1
HQ Space Division P.O. Box 92960 World Way Postal Center Los Angeles, California 90009 ATTN: YGJ, COL Kennedy	1
HQ USAF/INES Pentagon Washington, D.C. 20330 ATTN: COL Sherman	1
HQ USAF/RDSD Pentagon Washington, D.C. 20330 ATTN: LTC Mittelman	1
HQ USAF/SASM Pentagon Washington, D.C. 30030 ATTN: CPT Kolter	1
HQ USAF/XOO Pentagon Washington, D.C. 20330	1
HQ USAF/XOK Pentagon Washington, D.C. 20330	1
HQ U.S. Navy/NOP009 Pentagon Washington, D.C. 20350	1
Analytic Services, Inc. 400 Army-Navy Drive Arlington, Virginia 22202 ATTN: Charles L. Smith	1

DL-3

UNCLASSIFIED

UNCLASSIFIED

DISTRIBUTION LIST - Concluded (U)

<u>Names and Addresses</u>	<u>Number of Copies</u>
MIT/Lincoln Laboratory P.O. Box 73 Lexington, Massachusetts 02173 ATTN: GP37, Ken Roth	1
The MITRE Corporation Box 208 Bedford, Massachusetts 01730 ATTN: Paul Schubert, M.S. B151	1

DL-4

UNCLASSIFIED